

# 1 Simulating Secondary Organic Aerosol in a Regional Air 2 Quality Model Using the Statistical Oxidation Model: 2. 3 Assessing the Influence of Vapor Wall Losses

4  
5 **Christopher D. Cappa<sup>1,\*</sup>, Shantanu H. Jathar<sup>2</sup>, Michael J. Kleeman<sup>1</sup>, Kenneth S.  
6 Docherty<sup>3</sup>, Jose L. Jimenez<sup>4</sup>, John H. Seinfeld<sup>5</sup>, Anthony S. Wexler<sup>1</sup>**

7 [1] Department of Civil and Environmental Engineering, University of California, Davis, CA,  
8 USA

9 [2] Department of Mechanical Engineering, Colorado State University, Fort Collins, CO, USA

10 [3] Alion Science and Technology, Research Triangle Park, NC, USA

11 [4] Cooperative Institute for Research in Environmental Sciences and Department Chemistry and  
12 Biochemistry, University of Colorado, Boulder, CO, USA

13 [5] Division of Chemistry and Chemical Engineering and Division of Engineering and Applied  
14 Science, California Institute of Technology, Pasadena, CA, USA

15 Correspondence to: C. D. Cappa (cdcappa@ucdavis.edu)

## 16 17 **1 Abstract**

18 The influence of losses of organic vapors to chamber walls during secondary organic aerosol  
19 (SOA) formation experiments has recently been established. Here, the influence of such losses on  
20 simulated ambient SOA concentrations and properties is assessed in the UCD/CIT regional air  
21 quality model using the statistical oxidation model (SOM) for SOA. The SOM was fit to laboratory  
22 chamber data both with and without accounting for vapor wall losses following the approach of  
23 Zhang et al. (2014). Two vapor wall loss scenarios are considered when fitting of SOM to chamber  
24 data to determine best-fit SOM parameters, one with “low” and one with “high” vapor wall-loss  
25 rates to approximately account for the current range of uncertainty in this process. Simulations  
26 were run using these different parameterizations (scenarios) for both the southern California/South  
27 Coast Air Basin (SoCAB) and the eastern United States (US). Accounting for vapor wall losses  
28 leads to substantial increases in the simulated SOA concentrations from VOCs in both domains,  
29 by factors of ~2-5 for the low and ~5-10 for the high scenario. The magnitude of the increase scales  
30 approximately inversely with the absolute SOA concentration of the no loss scenario. In SoCAB,  
31 the predicted SOA fraction of total OA increases from ~0.2 (no) to ~0.5 (low) and to ~0.7 (high),

32 with the high vapor wall loss simulations providing best general agreement with observations. In  
33 the eastern US, the SOA fraction is large in all cases but increases further when vapor wall losses  
34 are accounted for. The total OA/ $\Delta$ CO ratio captures the influence of dilution on SOA  
35 concentrations. The simulated OA/ $\Delta$ CO in SoCAB (specifically, at Riverside, CA) is found to  
36 increase substantially during the day only for the high vapor wall loss scenario, which is consistent  
37 with observations and indicative of photochemical production of SOA. Simulated O:C atomic  
38 ratios for both SOA and for total OA increase when vapor wall losses are accounted for, while  
39 simulated H:C atomic ratios decrease. The agreement between simulations and observations of  
40 both the absolute values and the diurnal profile of the O:C and H:C atomic ratios for total OA was  
41 greatly improved when vapor wall-losses were accounted for. These results overall demonstrate  
42 that vapor wall losses in chambers have the potential to exert a large influence on simulated  
43 ambient SOA concentrations, and further suggest that accounting for such effects in models can  
44 explain a number of different observations and model/measurement discrepancies.

45

## 46 **2 Introduction**

47 Particulate organic matter, or organic aerosol (OA), is derived from primary emissions or from  
48 secondary chemical production in the atmosphere from the oxidation of volatile organic  
49 compounds (VOCs). OA makes up a substantial fraction of atmospheric submicron particulate  
50 matter (Zhang et al., 2007), influencing the atmospheric fate and impact of PM on regional and  
51 global scales. Gas-phase oxidation of VOCs leads to the formation of oxygenated product species  
52 that can condense onto existing particles or nucleate with other species to form new particles (e.g.  
53 Ziemann and Atkinson, 2012). Much of the understanding regarding the formation of secondary  
54 organic aerosol (SOA) via condensation has been derived from experiments conducted in  
55 laboratory chambers. In a typical experiment, a precursor VOC is added to the chamber and  
56 exposed to an oxidant (e.g. OH, O<sub>3</sub> or NO<sub>3</sub>). As both the precursor VOC and the oxidation products  
57 react with the oxidant, SOA is formed. The amount of SOA formed per amount of precursor  
58 reacted (i.e. the SOA mass yield) can then be quantified (e.g. Odum et al., 1996). Such SOA yield  
59 measurements form the basis of most parameterizations of SOA formation in regional air quality  
60 and global chemical-transport and climate models (Tsigaridis et al., 2014). However, too often  
61 simulated SOA concentrations underestimate observed values, especially in polluted regions, and  
62 sometimes dramatically so (Heald et al., 2005; Volkamer et al., 2006; Ensberg et al., 2013). There  
63 have been various efforts to account for model/measurement disparities including, most notably:  
64 (i) the addition of new SOA precursors in the form of so-called semi-volatile and intermediate  
65 volatility organic compounds, S/IVOCs, including treating primary organic aerosol as semi-  
66 volatile (Robinson et al., 2007); (ii) the addition of ad hoc “ageing” schemes on top of existing  
67 parameterizations of SOA from VOCs (Lane et al., 2008b; Tsimpidi et al., 2010; Dzepina et al.,  
68 2011); (iii) updating of aromatic SOA yields (Dzepina et al., 2009); and (iv) production of SOA in the aqueous phase in aerosol-water, clouds  
69 and fogs (Ervens et al., 2011). More recently, concerns over the influence of vapor wall losses on the  
70 experimental chamber data used to develop the parameterizations have arisen (Matsunaga and  
71 Ziemann, 2010; Zhang et al., 2014). The influence of erroneously low SOA yields due to vapor  
72 wall losses on simulated SOA concentrations in three-dimensional regional models and properties  
73 is the focus of the current work.

74 Recent observations have demonstrated that organic vapors can be lost to Teflon chamber  
75 walls, and that the extent of loss is related to the compound vapor pressures with lower vapor  
76 pressure compounds partitioning more strongly to the walls than higher vapor pressure compounds

77 (Matsunaga and Ziemann, 2010; Kokkola et al., 2014; Krechmer et al., 2015; Yeh and Ziemann,  
78 2015; Zhang et al., 2015). These results suggest that vapor wall losses during SOA formation  
79 experiments could potentially bias observed SOA concentrations. Indeed, Zhang et al. (2014)  
80 observed that SOA yields from toluene + OH photooxidation depend explicitly on the seed particle  
81 surface area, all other conditions being equal. They interpreted these observations using a dynamic  
82 model of particle growth coupled with a parameterizable gas-phase chemical mechanism, the  
83 statistical oxidation model (SOM) (Cappa and Wilson, 2012). They determined that substantial  
84 vapor wall losses were most likely the cause of this dependence, with biases of up to a factor of  
85  $\sim 4$  for these experiments. Further, they estimated for this system that the vapor wall loss rate  
86 coefficient ( $k_{\text{wall}}$ ) was  $\sim 2 \times 10^{-4} \text{ s}^{-1}$  for their  $25 \text{ m}^3$  chamber. This value of  $k_{\text{wall}}$  is in reasonable  
87 agreement both with theoretical expectations—so long as the vapor-wall accommodation  
88 coefficient ( $\alpha_{\text{wall}}$ ) is  $> 10^{-5}$ —and with results of Ziemann and colleagues (Matsunaga and Ziemann,  
89 2010; Yeh and Ziemann, 2015) who estimated  $k_{\text{wall}} \sim 6 \times 10^{-4} \text{ s}^{-1}$  for their  $8 \text{ m}^3$  chamber. Kokkola  
90 et al. (2014) have also suggested vapor wall losses can impact SOA yields, although they  
91 determined a much larger  $k_{\text{wall}}$  of  $\sim 10^{-2} \text{ s}^{-1}$  for their  $4 \text{ m}^3$  chamber. Recent direct measurements of  
92  $k_{\text{wall}}$  for a range of oxidized VOCs (OVOCs), produced from reactions of VOCs in traditional  
93 chambers, suggest that  $k_{\text{wall}}$  can vary by an order of magnitude ( $\sim 2 \times 10^{-6} - 3 \times 10^{-5} \text{ s}^{-1}$ ) and that  
94  $k_{\text{wall}}$  is dependent on the OVOC vapor pressure (Zhang et al., 2015); such low  $k_{\text{wall}}$  values implies  
95 that the  $\alpha_{\text{wall}}$  is  $< 10^{-5}$  and controls the rate of vapor loss to the walls.

96 Although the exact value of  $k_{\text{wall}}$  is likely chamber-specific (which likely contributes to some  
97 of the above-mentioned variability in  $k_{\text{wall}}$ ) and thus the exact influence of vapor wall losses on  
98 chamber SOA measurements remains somewhat uncertain, the preponderance of evidence  
99 suggests that such effects are important. Existing SOA parameterizations have typically not been  
100 determined with explicit accounting for vapor wall losses. Consequently, they likely underestimate  
101 actual SOA formation in the atmosphere where walls are much less important (although dry  
102 deposition of vapors may still be a factor (Hodzic et al., 2014)). Two recent efforts have attempted  
103 to estimate the influence of vapor wall losses on SOA concentrations in the atmosphere (Baker et  
104 al., 2015; Hayes et al., 2015). One of the studies (Baker et al., 2015) builds on the existing two-  
105 product parameterization of SOA formation in the Community Multiscale Air Quality (CMAQ)  
106 model and simply scales the yields of the semi-volatile products up by factors of 4. In the two-  
107 product model, a given VOC reacts to form two semi-volatile products that partition to the

108 condensed phase. The semi-volatile products are formed with mass yields,  $y_i$ , and partitioning  
109 coefficients,  $K_i$ , that have been determined by fitting the model to data from chamber experiments  
110 in which vapor wall losses were not accounted for. The other study (Hayes et al., 2015) used a  
111 similar yield-scaling approach, but within the volatility basis set (VBS) four-product framework  
112 to represent SOA formation, and they scaled the mass yields for only the semi-volatile product  
113 species from aromatics. Not surprisingly, these simple *ad hoc* scaling methods demonstrated that  
114 increasing the yields of the semi-volatile products from their originally parameterized values  
115 increases the simulated SOA concentration, but quantitative interpretation of the results is difficult.  
116 This is an especially important consideration given that different SOA systems may exhibit  
117 different sensitivities to vapor wall losses, owing to differences in the product species volatility  
118 distribution and the extent to which multi-generational ageing influences the SOA formation. More  
119 robust assessment of the influence of vapor wall losses on simulated SOA concentrations in  
120 regional air quality models is thus needed.

121 In this study, the SOM SOA model (Cappa and Wilson, 2012) is utilized to examine the  
122 influence of vapor wall losses on simulated SOA concentrations and O:C atomic ratios in a 3D  
123 regional air quality model, specifically the UCD/CIT (Kleeman and Cass, 2001). What  
124 distinguishes the present approach is that the potential influence of vapor wall losses is inherently  
125 accounted for during the development of the SOM SOA parameterization (Zhang et al., 2014).  
126 This can be contrasted with a simple scaling of an existing parameterization. The current approach  
127 allows for more detailed characterization of different precursor species, reaction conditions (e.g.  
128  $\text{NO}_x$  sensitivities) and the complex interplay of various timescales (reaction, gas/wall partitioning  
129 and gas/particle partitioning). This also allows for examination of the extent to which different  
130 assumptions regarding the value of  $k_{\text{wall}}$  (i.e. the first-order rate constant for vapor loss to chamber  
131 walls) during development of the SOA parameterization impact simulations of ambient SOA  
132 concentrations. Further, the SOM framework simulates O:C atomic ratios in addition to OA mass  
133 concentrations, and thus allows for more detailed assessment of the simulated OA and comparison  
134 with observations. Our results demonstrate that accounting for vapor wall losses can have a  
135 substantial impact on simulated SOA concentrations and suggest that there may be regionally-  
136 specific differences.

137

## 138 **3 Methods**

### 139 **3.1 Air quality model**

140 Regional air quality simulations were performed using the UCD/CIT chemical transport model  
141 (Kleeman and Cass, 2001) for two geographical domains: (i) the Southern California Air Basin  
142 (SoCAB) and (ii) the eastern US. Details regarding the general model configuration and emissions  
143 inventory used have been previously discussed (Jathar et al., 2015a), and the reader is referred to  
144 that work for further information. Details specific to the current work are provided in the following  
145 sections. Model simulations were run for SoCAB from July 20 to August 2, 2005 and for the  
146 eastern US from August 20 to September 2, 2006. Model spatial resolution was higher in SoCAB  
147 (8 km x 8 km) than in the eastern US (36 km x 36 km) to account for the different domain sizes.

### 148 **3.2 Statistical Oxidation Model for SOA**

149 SOA formation from six VOC classes was simulated using the statistical oxidation model  
150 (Cappa and Wilson, 2012; Cappa et al., 2013), which was recently implemented in the UCD/CIT  
151 model (Jathar et al., 2015a). The VOC classes considered are: long alkanes, benzene, high-yield  
152 aromatics (i.e. toluene), low-yield aromatics (i.e. m-xylene), isoprene and terpenes (including both  
153 mono- and sesquiterpenes). SOM is a parameterizable model that simulates the multi-generational  
154 oxidation of the product species formed from reaction of the SOA precursor VOCs. In SOM, a  
155 “species” is defined as a molecule with a specific number of carbon and oxygen atoms ( $N_C$  and  
156  $N_O$ , respectively), and where the VOC-specific properties of these SOM species are determined  
157 through fitting to laboratory observations. Reactions of a SOM species lead to either  
158 functionalization (i.e. addition of oxygen atoms while conserving the number of carbon atoms) or  
159 fragmentation (i.e. the production of two species which individually have fewer carbon atoms but  
160 where the total carbon is conserved, and where each new species adds one additional oxygen  
161 atom). The particular tunable parameters in SOM are: the probability of adding one, two, three or  
162 four oxygen atoms per reaction, referred to as  $p_{XO}$ ; the decrease in vapor pressure per added  
163 oxygen, referred to as  $\Delta LVP$ ; and the probability of fragmentation, which is related to the O:C  
164 atomic ratio of a given species as  $P_{frag} = (O:C)^{m_{frag}}$  and where  $m_{frag}$  is the tunable parameter.  
165 SOA formation from the semi-volatile SOM species assumes that partitioning is described  
166 according to absorptive gas-particle partitioning theory (Pankow, 1994), and the gas-particle mass

167 transfer has been simulated using dynamic partitioning (Kleeman and Cass, 2001; Zhang et al.,  
168 2014; Jathar et al., 2015a). The parameters used in the current work have been determined by  
169 fitting to time-dependent data from SOA formation experiments conducted in the Caltech chamber  
170 both with and without accounting for vapor wall losses during the fitting process (discussed further  
171 below); references for the specific experiments considered are provided in Table S1. The specific  
172 influence of considering multi-generational ageing on simulated SOA concentrations and  
173 properties is discussed in a companion paper (Jathar et al., 2015b). The use of the SOM to represent  
174 SOA formation leads to an increase of about a factor of 2.5 or less in computer processing time  
175 required compared to use of the 2-product model.

### 176 **3.3 Accounting for Vapor Wall Loss**

#### 177 **3.3.1 SOM**

178 Vapor wall losses have been accounted for using SOM, as detailed in Zhang et al. (2014).  
179 Vapor wall loss is treated as a reversible, absorptive process with vapor uptake specified using a  
180 first-order rate coefficient ( $k_{\text{wall}}$ ) and the desorption rate related to the effective saturation  
181 concentration,  $C^*$ , of the organic species and the effective absorbing mass of the walls (Matsunaga  
182 and Ziemann, 2010). Unique SOM fits (i.e. values of  $m_{\text{frag}}$ ,  $\Delta\text{LVP}$  and  $p_{\text{XO}}$ ) have been determined  
183 for different assumed values of  $k_{\text{wall}}$ . Best-fit values are provided in Table S1. It should be noted  
184 that the influence of vapor wall losses is inherent in the fit parameters, and in the absence of walls  
185 (i.e. in the atmosphere) the predicted SOA formed will be larger when the fits account for vapor  
186 wall losses. A base case set of parameters with no vapor wall losses assumed during fitting (termed  
187 SOM-no) was determined using  $k_{\text{wall}} = 0$ . In Zhang et al. (2014), an optimal value of  $k_{\text{wall}} = 2 \times 10^{-4}$   
188  $\text{s}^{-1}$  was determined for the California Institute of Technology chamber based on simultaneous  
189 fitting of the SOM to a set of toluene photooxidation experiments conducted at different seed  
190 particle concentrations. Unlike in Zhang et al. (2014), the values of  $k_{\text{wall}}$  used here were not  
191 determined during model fitting. This is because the absolute value of  $k_{\text{wall}}$  is not well constrained  
192 by a single experiment, and the simulations require vapor wall loss corrected parameters for VOCs  
193 besides toluene. Therefore, two specific bounding cases that account for vapor wall loss are instead  
194 considered based on the results from Zhang et al. (2014). Specifically, values of  $k_{\text{wall}} = 1 \times 10^{-4} \text{ s}^{-1}$

195 and  $2.5 \times 10^{-4} \text{ s}^{-1}$  are considered, corresponding to a low vapor wall loss case (SOM-low) and high  
196 vapor wall loss case (SOM-high), respectively.

197 An important aspect of vapor wall loss is that the impact it has on SOA concentrations is  
198 dependent upon the timescale associated with vapor-particle equilibration ( $\tau_{v-p}$ ) (McVay et al.,  
199 2014; Zhang et al., 2014). The  $\tau_{v-p}$  is related to the accommodation coefficient associated with  
200 vapor condensation on particles,  $\alpha_{\text{particle}}$ . Above a vapor-particle accommodation coefficient of  
201  $\alpha_{\text{particle}} \sim 0.1$  variations in the exact value of  $\alpha_{\text{particle}}$  does not influence the effects of vapor wall  
202 losses. This is not to say that vapor wall losses have no influence on the amount of SOA formed  
203 when  $\alpha_{\text{particle}} \geq 0.1$ , only that the net impact does not depend on  $\alpha_{\text{particle}}$ . Below this value, vapor-  
204 particle equilibration is slowed and the effects of loss of vapors to the walls are accentuated. Thus,  
205 a conservative estimate that minimizes the influence of vapor wall losses on SOA formation is  
206 obtained using  $\alpha_{\text{particle}} \geq 0.1$ . Here, data fitting and parameter determination was performed  
207 assuming that  $\alpha_{\text{particle}} = 1$ , and is thus a conservative estimate.

208 SOM was fit to time-dependent SOA formation experiments conducted in the California  
209 Institute of Technology chamber, following the methodologies described in Cappa et al. (2013)  
210 and Zhang et al. (2014). Observed suspended particle concentrations have been corrected only for  
211 physical deposition on chamber walls, which is appropriate since vapor wall losses are accounted  
212 for separately by SOM. Best-fit values for the SOM parameters for the base case (SOM-no) are  
213 given in Jathar et al. (2015a) and values for SOM-low and SOM-high determined here are given  
214 in Table S1, along with the sources of the experimental data. Parameters have been separately  
215 determined for experiments conducted under low- $\text{NO}_x$  and high- $\text{NO}_x$  conditions since the SOA  
216 yields differ. Example results that illustrate the influence of vapor wall losses on simulated SOA  
217 yields are presented in Figure S1 for box model simulations that have been conducted using the  
218 best-fit parameters determined for toluene SOA (low- $\text{NO}_x$  conditions), but where the simulations  
219 are run assuming there are no walls (i.e. by setting  $k_{\text{wall}} = 0$ ).

### 220 3.3.2 Two-product model

221 Ideally, SOA levels from the SOM-based simulations can be compared with similar results  
222 based on the commonly used two-product model. To do so involves determining new parameters  
223 for the two-product model in which vapor wall losses are explicitly accounted for. Therefore, vapor

224 wall-loss corrected SOA yield curves (i.e. [SOA] versus [ $\Delta$ HHC], where  $\Delta$ HHC is the concentration  
225 of reacted hydrocarbon) were generated with SOM using the parameters determined by fitting  
226 SOM to the original chamber data when  $k_{\text{wall}} > 0$ , but now where  $k_{\text{wall}}$  is set to zero. The 2-product  
227 model could then be fit to these “corrected” yield curves to determine vapor wall-loss corrected  
228 yields and partitioning coefficients. These new fits would inherently account for the influence of  
229 vapor wall loss since the two-product model is being fit to the corrected “wall-less” data and thus  
230 differ from *ad hoc* scaling of yields. However, it was determined that the two-product fits were  
231 not sufficiently robust across the entire suite of compounds and vapor wall loss conditions  
232 considered to be implemented in the atmospheric model. An example for SOA from dodecane +  
233 OH under low-NO<sub>x</sub> reaction conditions is shown in Figure S2. We have determined that this lack  
234 of robustness is a result of the limited dynamic range of the 2-product model. This can be  
235 contrasted with the SOM, which includes many more species that span a wider, more continuous  
236 volatility range, making it more flexible when fitting the laboratory data. More specifically, the  
237 SOA concentrations from the chamber observations, both uncorrected and corrected, ranged from  
238  $\sim 1\text{-}500 \mu\text{g m}^{-3}$ , often with few data points at concentrations less than  $\sim 10 \mu\text{g m}^{-3}$ . Thus, when fits  
239 were performed, inconsistent behavior between the different vapor wall loss conditions was  
240 obtained over the atmospherically relevant concentration range ( $\sim 0.1\text{-}20 \mu\text{g m}^{-3}$ ). Attempts were  
241 made to fit the two-product model over a restricted concentration range or to fit using  $\log([\text{SOA}])$   
242 instead of [SOA]. However, neither effort led to sufficiently robust results (although both did lead  
243 to improvements). This null result suggests that simple scaling of two-product yields (Baker et al.,  
244 2015) to account for the effects of vapor wall losses may not be appropriate. This may similarly  
245 apply to scaling of VBS parameters (Hayes et al., 2015), although the greater flexibility of the  
246 VBS (commonly implemented with four products, instead of two) can potentially allow for unique  
247 “wall-less” fits to be determined (Hodzic et al., 2015). The extent to which such alternative  
248 methods can robustly account for vapor wall losses that are computationally less intensive than  
249 SOM will be explored in future work.

### 250 **3.4 Primary Organic Aerosol and IVOCs**

251 Primary organic aerosol (POA) derived from anthropogenic (e.g. vehicular activities, food  
252 cooking) or pyrogenic (e.g. wood combustion) sources are simulated assuming that the POA is  
253 non-volatile. This is the standard assumption in the CMAQ model framework (Simon and Bhawe,

254 2011), and thus is adopted here. It is known that some POA is semi-volatile, not non-volatile as  
255 assumed here. Had POA been treated within a semi-volatile framework (Robinson et al., 2007),  
256 such that some fraction of the POA can evaporate (i.e. SVOCs) and react within the gas-phase and  
257 be converted to SOA (sometimes improperly referred to as “oxidized POA”), then the amount of  
258 POA would likely decrease (due to evaporation) and the amount of simulated SOA would increase  
259 (due to condensation of oxidized SVOC vapors); the total OA concentration (POA + SOA) may  
260 or may not increase as a result, depending on the details of the parameterization and the  
261 atmospheric conditions. Additionally, nearly all modeling efforts in which POA is treated as semi-  
262 volatile have also included contributions from gas-phase IVOCs as an added class of SOA  
263 precursors; these two issues are rarely implemented independently in models, although their  
264 contributions can be separately tracked. Whereas simply treating POA as semi-volatile may or  
265 may not lead to an increase in the total OA concentration, the introduction of new SOA precursor  
266 mass in the form of IVOCs will inevitably lead to production of more SOA in the model. The  
267 relative importance of IVOCs will depend on the amount of added IVOC mass and the propensity  
268 of these IVOC vapors to form SOA in the model (i.e. their effective SOA yield). In the current  
269 study, we do not explicitly consider the potential for IVOCs to contribute to the ambient SOA  
270 burden, focusing instead on how vapor wall losses influence SOA formation from VOCs. We will  
271 aim to consider contributions from IVOCs and how they are influenced by vapor wall losses in  
272 future studies. Regardless, the implications of our particular treatment (non-volatile POA  
273 excluding IVOCs) are discussed below.

### 274 **3.5 Model Simulations and Outputs**

275 Six individual model simulations have been carried out to determine the spatial distribution of  
276 SOA concentrations. Each simulation used one of the SOM parameterizations, i.e. SOM-no, SOM-  
277 low or SOM-high with either the low- and high-NO<sub>x</sub> parameters. Each precursor VOC is allowed  
278 to react with either OH, O<sub>3</sub> or NO<sub>3</sub> as characterized by an oxidant-specific rate coefficient,  
279 although the products and product distributions of the first-generation products are assumed to be  
280 oxidant independent. This simplification is identical to that employed in CMAQv4.7 (Carlton et  
281 al., 2010). Reactions of subsequent oxidized SOM products then occur only via reaction with OH  
282 radicals according to the SOM parameterization associated with that precursor VOC (as  
283 determined by fitting the photooxidation experiments). Besides the absolute SOA concentration,

284 SOM also allows for explicit calculation of the average (and precursor-specific) O:C and H:C  
285 atomic ratios and of the SOA volatility distribution, which characterizes the distribution of  
286 particulate and gas-phase mass concentrations with respect to  $C^*$ . To estimate the O:C of the total  
287 OA (POA + SOA), it is assumed that the non-volatile POA has a constant O:C = 0.2 and H:C =  
288 2.0 (Ng et al., 2011). Since the simulated  $(O:C)_{total}$  is just a combination of  $(O:C)_{SOA}$  and  $(O:C)_{POA}$ ,  
289 assuming a different value for  $(O:C)_{POA}$  would change the absolute value of  $(O:C)_{total}$  but not any  
290 dependence on simulation conditions. This is similarly true for  $(H:C)_{total}$ .

291 As noted above, unique sets of SOM parameters were fit to experiments conducted under either  
292 low- or high- $NO_x$  conditions assuming a particular value for  $k_{wall}$ . Since each simulation used a  
293 single set of SOM fit parameters (e.g. SOM-no fit to low- $NO_x$  experiments) the SOA  $NO_x$   
294 parameterization used in a given simulation is independent of the actual simulated ambient  $NO_x$   
295 concentrations or  $NO/HO_2$  ratio. Consequently, comparison between the simulations conducted  
296 using the low- and high- $NO_x$  parameterizations gives an indication of the range expected from  
297 variability in  $NO_x$  levels, and the average between the two simulations provides a representation  
298 that is intermediate between these two extremes. Unless otherwise specified, reported values are  
299 for the average of the simulations run using the low- and high- $NO_x$  parameterizations. This  
300 approach towards understanding the influence of  $NO_x$  is different than some previous approaches  
301 that attempted to account for the SOA  $NO_x$  dependence in a more continuously variable manner.  
302 For example, some simulations using the two-product approach have used the instantaneous  
303  $NO/HO_2$  ratios predicted by the model to allow distinguishing between low- and high- $NO_x$   
304 products and SOA yields for aromatic VOCs (Carlton et al., 2010). Similarly, instantaneous  
305  $VOC/NO_x$  ratios have been used with VBS-type models for aromatic VOCs to allow for  
306 interpolation between the two regimes (Lane et al., 2008a). Typically, these efforts have not  
307 considered the  $NO_x$ -dependence of monoterpene and sesquiterpene yields even though it is  
308 experimentally established that the  $NO_x$  condition (and more specifically, the  $NO/HO_2$  ratio)  
309 influences SOA yields for both aromatic and biogenic compounds (e.g. Ng et al., 2007a; Ng et al.,  
310 2007b). For most VOCs, the functional dependence of the SOA yield on the  $VOC/NO_x$  ratio or the  
311  $NO/HO_2$  ratio is not well established, making it difficult to understand how well the interpolation  
312 methods work. (SOA formation from isoprene is a notable exception (e.g. Xu et al., 2014).)  
313 Further, modeled  $NO/HO_2$  ratios may be off by orders of magnitude, most likely due to poor  
314 representation of  $HO_2$  concentrations (Carlton et al., 2010), making it difficult to understand how

315 well the conditions of the laboratory translate to the model environment. By considering the low-  
316 and high-NO<sub>x</sub> parameterizations separately, i.e. the approach used in the current study, bounds on  
317 the overall influence of NO<sub>x</sub> on the simulated SOA can be established. However, this approach  
318 will not capture how the simulated SOA may vary due to spatial and temporal variations in the  
319 model NO<sub>x</sub> and oxidant fields. Future efforts will aim to account for the NO<sub>x</sub>-dependence of SOA  
320 formation in a more continuously varying manner, and to account for recent updates to the detailed  
321 isoprene oxidation mechanism (Pye et al., 2013).

## 322 **4 Results and Discussion**

### 323 **4.1 General influence of vapor wall loss on simulated SOA**

324 The spatial distribution of the SOM-no model SOA concentrations is shown for SoCAB and  
325 the eastern US using the average from the simulations carried out using the low- and high-NO<sub>x</sub>  
326 parameterizations (Figure 1a-b). (Again, the low- and high-NO<sub>x</sub> designations here refer only to the  
327 experimental conditions under which the SOM parameters were determined, not the actual NO<sub>x</sub>  
328 conditions in the UCD/CIT model.) For SoCAB, predicted SOA concentrations are largest in and  
329 around downtown Los Angeles and in the forested regions of the Los Padres National Forest and  
330 the Santa Monica Mountains National Recreation Area in the NW quadrant. The spatial  
331 distribution of SOA is similar to that obtained using the conventional two-product SOA  
332 parameterization (Jathar et al., 2015a, b). For the eastern US, predicted SOA concentrations are  
333 largest in the southeast, in particular around Atlanta, Georgia. Overall, the simulated SOA  
334 concentrations with the SOM-no model are larger in the eastern US than in SoCAB, reflecting the  
335 relatively strong influence of biogenic emissions in this region.

336 The influence of vapor wall losses on the simulated ambient SOA concentrations is illustrated  
337 in Figure 1c-f as the ratio between the SOA from the SOM-low and SOM-high simulations to the  
338 SOM-no (no wall losses) simulation. This ratio will be referred to generally as the wall loss impact  
339 ( $R_{\text{wall,low}}$  or  $R_{\text{wall,high}}$ ). Values of  $R_{\text{wall}}$  larger than one indicate that accounting for vapor wall losses  
340 as part of the SOM parameterization leads to an increase in the predicted SOA concentrations. In  
341 the SoCAB, the  $R_{\text{wall,low}}$  varies from 1.5-4.5, while the  $R_{\text{wall,high}}$  varies from 3 to more than 10. The  
342 largest ratios (indicating the largest impact of accounting for vapor wall losses) tend to occur in  
343 more remote locations as this is where concentrations are lower (Figure 2). However, the impact

344 is still large in downtown Los Angeles and the greater LA region (average  $R_{\text{wall,low}} \sim 2.5$  and  $R_{\text{wall,high}}$   
345  $\sim 5$ ). In the eastern US, the simulated  $R_{\text{wall}}$  vary over a similar range as in SoCAB, with  $R_{\text{wall,low}}$   
346 varying from 1.5-5 and  $R_{\text{wall,high}}$  from 3 to 10. There is again a general, although not exact, inverse  
347 relationship between  $R_{\text{wall}}$  and the absolute SOA concentrations; the greater scatter in the eastern  
348 US compared to SoCAB at low SOA concentrations likely reflects the larger spatial range  
349 considered. The smallest simulated  $R_{\text{wall}}$  values occur across the southeast and up the eastern  
350 seaboard ( $R_{\text{wall,low}} \sim 2.5$  and  $R_{\text{wall,high}} \sim 5$ ) while the largest values occur over the Great Lakes and  
351 Michigan, Nebraska, and the Gulf of Mexico and Atlantic Ocean; there is a steep increase going  
352 from land to sea. If  $R_{\text{wall}}$  values are calculated using the simulated SOA concentrations from either  
353 the low- $\text{NO}_x$  or high- $\text{NO}_x$  parameterizations individually, as opposed to the average values used  
354 above, very similar results are obtained (Figure S3).

355 Regional air quality models have historically overestimated the urban-to-regional gradient in  
356 total OA concentrations. Robinson et al. (2007) showed that the simulated urban-to-regional  
357 gradient could be reduced and made more consistent with observations by treating POA as semi-  
358 volatile and adding SVOCs and IVOCs as SOA-forming species. The current results suggest a  
359 complementary explanation, namely that the urban-to-regional gradient can be reduced when  
360 vapor wall losses are accounted for since  $R_{\text{wall}}$  generally increases with decreasing SOA  
361 concentration and since POA is identical between the different model parameterizations.  
362 Consequently, larger  $R_{\text{wall}}$  are found outside of the major source regions, which decreases the  
363 urban-to-regional contrast. Indeed, the ratio between the predicted average SOA in downtown LA  
364 (urban) to that over the Pacific Ocean near the coast of LA (regional) and decreases from 2.3  
365 (SOM-no) to 1.5 (SOM-low) to 1.3 (SOM-high), for example. Additionally, it has been suggested  
366 that the typical underprediction of SOA by air quality and chemical transport models relative to  
367 observations might increase with photochemical age (Volkamer et al., 2006). The current results  
368 suggest the possibility that the SOA concentrations in more remote (lower concentration) regions  
369 may be underestimated in models to a greater extent in a relative sense than in high-source (higher  
370 concentration) regions due to a lack of accounting for vapor wall losses, although the absolute  
371 differences in SOA concentrations may be larger in regions where absolute concentrations are  
372 larger.

## 373 4.2 OA composition and concentrations

374 The simulated fraction of total OA that is SOA ( $f_{\text{SOA}}$ ) is substantially smaller in SoCAB than  
375 in the eastern US, especially the southeast US (Figure 3). The predicted  $f_{\text{SOA}}$  values vary spatially  
376 within a given region, with the SOM-no simulations in the general range of  $\sim 0.1$ - $0.3$  for SoCAB  
377 and  $\sim 0.4$ - $0.9$  for the eastern US. This difference between regions results from the substantial POA  
378 emissions in SoCAB and the large emissions of biogenic VOCs across the southeast US.  
379 Consequently, accounting for vapor wall losses has a larger impact on the absolute total OA (SOA  
380 + POA) concentrations in the eastern US than it does in SoCAB, although the impact in both  
381 regions is substantial. For SoCAB, the predicted 24-h average  $f_{\text{SOA}}$  range increases to  $\sim 0.2$ - $0.5$  for  
382 SOM-low and to  $\sim 0.4$ - $0.8$  for SOM-high simulations. These model results can be compared with  
383 measurements from the 2005 SOAR field study in Riverside, CA, which overlaps with the  
384 simulation period. The observed  $f_{\text{SOA}}$  during SOAR ranged from  $\sim 0.6$  in early morning to  $\sim 0.9$  in  
385 midday, with a campaign-average of  $\sim 0.78$  (Docherty et al., 2011). Measurements at Pasadena,  
386 CA during a later time period, June 2010 during the CalNex study, give similar results with the  
387 campaign-average  $f_{\text{SOA}} = 0.6$  (Hayes et al., 2013). (Note that here we are equating SOA with the  
388 “oxygenated organic aerosol,” or OOA factors that are obtained from positive matrix factorization  
389 of the measured OA time series, and equating POA with the sum of hydrocarbon-like OA (HOA),  
390 cooking-derived OA (COA), and “local” OA (LOA).) The SOM-high simulations in SoCAB are  
391 most consistent with these observations.

392 For the eastern US, the predicted  $f_{\text{SOA}}$  range increases from  $0.4$ - $0.9$  for SOM-no to  $\sim 0.7$ - $0.9$  for  
393 SOM-low and to  $\sim 0.8$ - $1$  for SOM-high. These predicted values can be compared with  
394 measurements made at a few locations in the southeastern US (specifically, sites in Alabama and  
395 Georgia), which show that the  $f_{\text{SOA}}$  in this region exhibits a strong seasonal dependence and some  
396 spatial variation (Xu et al., 2015b). The measurements in spring and summer indicate that the total  
397 OA is dominated by SOA, with  $f_{\text{SOA}}$  measurements ranging from  $0.7$  to  $1$  and with the smaller  
398 values observed at the more urban sites. The predicted  $f_{\text{SOA}}$  from the SOM-low and SOM-high  
399 simulations are most consistent with this range, with the  $f_{\text{SOA}}$  from the SOM-no simulations being  
400 on the low side, especially in comparison with the more rural sites.

401 The simulated total OA concentrations are compared to ambient OA measurements made at  
402 the STN (Speciated Trends Network) and IMPROVE (Interagency Monitoring of Protected Visual

403 Environments) (The Visibility Information Exchange Web System (VIEWS 2.0), 2015) air quality  
 404 monitoring sites in SoCAB and the eastern US; the regional differences in  $f_{SOA}$  should be kept in  
 405 mind for this model/measurement comparison. A map of sites is shown in Figure S4. STN sites  
 406 tend to be more urban and have higher OA concentrations compared to IMPROVE sites, which  
 407 tend to be more remote. OA concentrations are estimated as the measured organic carbon (OC)  
 408 concentrations times 2.1 for IMPROVE sites and as  $1.6 \times ([OC] - 0.5 \mu\text{g m}^{-3})$  for STN sites (Turpin  
 409 and Lim, 2001). The  $-0.5 \mu\text{g m}^{-3}$  offset for the STN sites arises because the IMPROVE data are  
 410 both artifact and blank corrected while the STN data are only artifact corrected (Subramanian et  
 411 al., 2004). The difference in scaling factors (2.1 versus 1.6) approximately accounts for differences  
 412 in the OA/OC conversion between more urban and more rural networks (Turpin and Lim, 2001).  
 413 Given the generally regional character of OA in much of the eastern US, it may be that the  
 414 difference in OM/OC between the STN and IMPROVE sites may be smaller than assumed here  
 415 (most likely with the 1.6 being too low, leading potentially to an underestimate in the OA at the  
 416 STN sites). We note that IMPROVE data may also be biased low by ~25% in the SE US summer  
 417 due to evaporation after sampling (Kim et al., 2015).

418 Table 1 lists statistical metrics of fractional bias, normalized mean square error (NMSE) and  
 419 the concordance correlation coefficients that capture model performance for OA for all simulations  
 420 for both domains across the STN and IMPROVE monitoring networks. Fractional bias is  
 421 calculated as:

$$422 \text{ Fractional bias} = \frac{2(C_{OA,sim} - C_{OA,obs})}{C_{OA,sim} + C_{OA,obs}} \quad (1)$$

423 and the NMSE as

$$424 \text{ NMSE} = \left| \frac{(C_{OA,sim} - C_{OA,obs})^2}{C_{OA,sim} \times C_{OA,obs}} \right| \quad (2)$$

425 where the subscripts *sim* and *obs* refer to the simulated and observed OA concentrations,  
 426 respectively. The concordance correlation coefficients ( $\rho_c$ ) are calculated as:

$$427 \rho_c = \frac{2s_{sim,obs}}{s_{sim}^2 + s_{obs}^2 + (\overline{C_{OA,sim}} - \overline{C_{OA,obs}})^2} \quad (3)$$

428 where  $\overline{C_{OA,sim}}$  and  $\overline{C_{OA,obs}}$  indicate the mean,  $s_{sim}^2$  and  $s_{obs}^2$  are the variance and  $s_{sim,obs}$  is the  
 429 covariance of the simulated and observed OA concentrations. Scatter plots are shown in Figure S5

430 and Figure S6; many more sites are considered in the eastern US than in the SoCAB given the  
431 larger geographical domain and distribution of sites. In both regions, the SOM-no simulations  
432 underpredict the STN and IMPROVE observations, especially in the SoCAB. The negative bias  
433 of the SOM-no simulations is generally improved as vapor wall losses are accounted for. For both  
434 the STN and IMPROVE sites in the SoCAB the SOM-high simulations give best agreement. For  
435 the eastern US STN sites, an average of the SOM-low and SOM-high simulations provides the  
436 best agreement. For the eastern US IMPROVE sites, the SOM-low simulations provide the best  
437 agreement, although with some overprediction. (If the eastern US STN and IMPROVE  
438 measurements do underestimate the actual OA concentrations, the degree to which accounting for  
439 vapor wall losses improves the model-measurement comparison will increase.) The simulated  
440 anthropogenic/biogenic SOA split is found to be approximately the same at sites within both  
441 networks (e.g. Figure 4). This occurs even though the IMPROVE sites tend to be more remote  
442 than the STN sites in the eastern US, and reflects the regional character of SOA in that region.  
443 Ultimately, the comparisons suggest that accounting for vapor wall losses can improve model-  
444 measurement agreement, although there are differences in terms of whether the SOM-high  
445 simulations or SOM-low simulations produce the best agreement. That the OA concentrations for  
446 the SOM-high simulations remains slightly lower than the observations for STN sites in SoCAB  
447 could potentially result from the non-volatile treatment of POA, the exclusion of IVOCs in the  
448 current model or uncertainty in the POA emission inventory.

449 The simulations can also be compared with observations of the OA-to- $\Delta$ CO concentration ratio  
450 (OA/ $\Delta$ CO) during SOAR (Docherty et al., 2008; Docherty et al., 2011), and where  $\Delta$ CO indicates  
451 the background corrected CO concentration. Because CO is relatively long lived, normalization of  
452 the calculated and observed OA to the concurrent background-corrected CO helps to minimize the  
453 impacts of uncertainties in boundary layer dynamics and accounts for variability in emissions and  
454 transport to some extent (De Gouw and Jimenez, 2009). The background-corrected CO  
455 concentration is calculated as  $\Delta[\text{CO}] = [\text{CO}] - [\text{CO}]_{\text{bgd}}$ . The estimated  $[\text{CO}]_{\text{bgd}}$  for the observations  
456 is 105 ppb (with a plausible range from 85-125 ppb) (Hayes et al., 2013). In contrast, the  $[\text{CO}]_{\text{bgd}}$   
457 for the model is estimated to be 130 ppb based on the simulated  $[\text{CO}]$  over the open ocean west of  
458 Los Angeles. The observed diurnal profile of OA/ $\Delta$ CO during SOAR exhibits a distinct peak  
459 around mid-day, corresponding to the peak in photochemical activity. This indicates a substantial  
460 influence of SOA production on the total OA concentration (Figure 5) (Docherty et al., 2008). The

461 simulated OA/ $\Delta$ CO diurnal profiles around Riverside for the SOM-high simulations are most  
462 consistent with the observations, exhibiting a distinct peak around mid-day that is similar to the  
463 observations (Figure 5). Unlike the observations, the diurnal OA/ $\Delta$ CO profile for the SOM-no  
464 simulation exhibits almost no increase during mid-day and the SOM-low simulation exhibits only  
465 a slightly larger daytime increase. The slope of a one-sided linear fit to a graph of the observed  
466 [OA] versus [CO] during daytime (10 am to 8 pm) is  $69 \pm 2 \mu\text{g m}^{-3} \text{ppm}^{-1}$  (Figure 5) when  
467 constrained to go through the assumed  $[\text{CO}]_{\text{bgd}}$ . This can be compared with the simulation results,  
468 which have constrained slopes of  $23.0 \pm 0.4$ ,  $34.0 \pm 0.8$  and  $55 \pm 2 \mu\text{g m}^{-3} \text{ppm}^{-1}$  for SOM-no,  
469 SOM-low and SOM-high, respectively (Figure 5g-i). Clearly the SOM-high simulations are in best  
470 overall agreement with the SOAR observations. However, the maximum in the simulated OA/ $\Delta$ CO  
471 peaks at a smaller value than was observed. The simulated peak also occurs slightly earlier than  
472 the maximum in the observations, which could be due to discrepancies in the transport to the  
473 Riverside site or to too fast SOA formation in the model. Nonetheless, these results clearly indicate  
474 that accounting for vapor wall losses has the potential to reconcile simulated SOA diurnal behavior  
475 with observations. Alternatively or complementarily, daytime increases in the OA/ $\Delta$ CO ratio from  
476 SOA production can be achieved with the introduction of additional SOA precursor material such  
477 as S/IVOCs (Zhao et al., 2014; Hayes et al., 2015), which are not considered here. The addition of  
478 S/IVOCs would increase the daytime OA/ $\Delta$ CO for all of the simulations. The magnitude of the  
479 increase would depend on the amount of added S/IVOCs and the properties assigned to the  
480 S/IVOCs regarding their SOA formation timescale and yield. Consideration of SOA from  
481 S/IVOCs in the SoCAB using the SOM framework will be the subject of future work.

## 482 **4.3 SOA Composition**

### 483 **4.3.1 Source/VOC Precursor Dependence**

484 Accounting for vapor wall losses leads to regionally-specific changes in the simulated  
485 contributions from the different VOC classes (e.g. TRP1, ARO1) to the SOA burden, as illustrated  
486 in Figure 4 for two sites in SoCAB (central Los Angeles and Riverside) and two in the eastern US  
487 (Atlanta and the Smoky Mountains). Focusing first on contributions from the biogenic VOCs, at  
488 all locations accounting for vapor wall losses leads to an increase in the fractional contribution of  
489 isoprene SOA, typically at the expense of terpene and sesquiterpene SOA. This is true for both the

490 low- and high-NO<sub>x</sub> simulations. Recent observations suggest that isoprene SOA produced via the  
491 low-NO IEPOX (isoprene epoxydiol) pathway can be uniquely identified from analysis of aerosol  
492 mass spectrometer measurements when the relative contribution is sufficiently large (> ~5%) (e.g.  
493 Budisulistiorini et al., 2013; Hu et al., 2015). This observed IEPOX SOA accounts for around 30%  
494 (May) and 40% (August) of total SOA or around 20% (May) and 30% (August) of total OA in  
495 Atlanta in the summer (Xu et al., 2015a), albeit not during the same time period as simulated here.  
496 IEPOX SOA was also found to account for 17% of total OA at a rural site in Alabama in 2013 (Hu  
497 et al., 2015). The SOM-low and SOM-high simulation results for Atlanta are most consistent with  
498 the observations, with a predicted isoprene SOA fraction of 27% and 35%, respectively, compared  
499 to only 17% for the SOM-no simulations and where the reported values are for the simulations that  
500 use the low-NO<sub>x</sub> parameterizations since this is the pathway that leads to IEPOX SOA. The related  
501 isoprene OA fractions are 10%, 21% and 31% for the SOM-no, -low and -high simulations,  
502 respectively. (These isoprene SOA fractions change only marginally for SOM-low and SOM-high  
503 simulations when the high-NO<sub>x</sub> parameterizations are used, to 25% and 37%, respectively. The  
504 SOM-no simulations exhibit somewhat greater sensitivity to the NO<sub>x</sub> parameterization, with the  
505 high-NO<sub>x</sub> parameterization giving an SOA fraction of 7%.)

506 In SoCAB, the predicted average isoprene SOA fraction in central LA is relatively large for  
507 the SOM-low (36%) and SOM-high (47%) simulations, compared to the SOM-no simulations  
508 (12%). There is a large difference in SoCAB between the simulations that use the low-NO<sub>x</sub> and  
509 high-NO<sub>x</sub> parameterizations, with the isoprene SOA fractions being much larger with the high-  
510 NO<sub>x</sub> parameterizations (e.g. 58% for high-NO<sub>x</sub> versus 36% for low-NO<sub>x</sub> for the SOM-high  
511 simulations). Measurements at Pasadena during the 2010 CalNex study did not distinctly identify  
512 IEPOX SOA, which is interpreted as the IEPOX SOA contribution being lower than ~5% of the  
513 OA (Hu et al., 2015). It is possible that additional isoprene SOA had been formed under higher  
514 NO<sub>x</sub> conditions (compared to the southeast US) such that it is chemically different from IEPOX-  
515 SOA and was not identified as a uniquely isoprene-derived SOA component, instead contributing  
516 generically to the overall oxygenated OA pool. The concentration of isoprene SOA from specific  
517 high-NO<sub>x</sub> pathways may, however, be limited at higher temperatures, such as found in  
518 summertime Pasadena, due to thermal decomposition of intermediate gas-phase species (Worton  
519 et al., 2013), although it is not clear to what extent this influenced the CalNex observations or  
520 would have affected the model results had it been explicitly considered. Additionally, it should be

521 kept in mind that the ambient NO<sub>x</sub> concentrations in SoCAB have decreased substantially from  
522 2005-2013 (Russell et al., 2012). Thus, although the CalNex measurements do not provide direct  
523 support for such a large isoprene SOA fraction, they also do not rule it out.

524 While the predicted isoprene SOA fraction increased, the predicted terpene and sesquiterpene  
525 SOA fractions decreased in the simulations that accounted for vapor wall losses. Additionally, the  
526 terpene SOA/sesquiterpene SOA ratio increased at all locations for the SOM-low and SOM-high  
527 simulations, in large part because the sesquiterpene yield is already large and thus accounting for  
528 vapor wall losses has a limited influence on the simulated sesquiterpene SOA concentrations.

529 There are some changes in the anthropogenic fraction of SOA when vapor wall losses are  
530 accounted for. The anthropogenic fraction of SOA is defined here as the sum of the SOA from  
531 long alkanes and aromatics, which are emitted from combustion of fossil fuels, divided by the sum  
532 of the total SOA, which additionally includes SOA from isoprene, monoterpenes and  
533 sesquiterpenes emitted by trees, plants and other natural sources. The <sup>14</sup>C isotopic signature of  
534 fossil-derived VOCs is different from that of biogenically derived VOCs, and thus their respective  
535 contributions to SOA can be partially constrained via experimental analysis of the <sup>14</sup>C content of  
536 OA (Zotter et al., 2014). We assume the anthropogenic fraction is equivalent to the fossil fraction  
537 of SOA (termed  $F_{\text{SOA,fossil}}$ ). At the two eastern US sites (Atlanta and Smokey Mountains) the  
538 average  $F_{\text{SOA,fossil}}$  increases slightly from 14% (SOM-no) to 22% (SOM-low) and 25% (SOM-  
539 high). At the two SoCAB sites (downtown LA and Riverside) the predicted average  $F_{\text{SOA,fossil}}$   
540 decreases slightly, from 35% (SOM-no) to 29% (SOM-low) and 30% (SOM-high), respectively.  
541 In SoCAB the  $F_{\text{SOA,fossil}}$  values differ between the low- and high-NO<sub>x</sub> parameterizations, with  
542  $F_{\text{SOA,fossil}}$  typically larger for the low-NO<sub>x</sub> parameterizations (e.g. 35% for low-NO<sub>x</sub> and 25% for  
543 high-NO<sub>x</sub>). In the eastern US, the predicted  $F_{\text{SOA,fossil}}$  exhibit a stronger response to vapor wall  
544 losses for the high-NO<sub>x</sub> parameterization than the low-NO<sub>x</sub> parameterization, although the  
545 absolute values are reasonably similar. Of the anthropogenic SOA (aromatics + alkanes), the high-  
546 NO<sub>x</sub> parameterizations indicate an increasing alkane SOA fraction as vapor wall losses are  
547 accounted for in both regions. In contrast, the low-NO<sub>x</sub> parameterizations indicate minor  
548 contributions from alkane SOA for all of the simulations. In general, chamber SOA yields from  
549 aromatic compounds are larger for low-NO<sub>x</sub> conditions (Ng et al., 2007a), which could help to  
550 explain these differences.

551 The SoCAB  $F_{SOA, fossil}$  values can be compared with estimates of the fossil fraction of “oxidized  
 552 organic carbon” ( $F_{OOC, fossil}$ ) from measurements made during CalNex in Pasadena (Zotter et al.,  
 553 2014). It should be noted that while  $F_{SOA, fossil}$  includes contributions from both oxygen and carbon  
 554 mass the  $F_{OOC, fossil}$  includes only the carbon mass. The fossil fraction of secondary organic carbon  
 555 (SOC) can be calculated from the simulated SOA concentrations by accounting for the differences  
 556 in the O:C atomic ratios of the different SOA types to facilitate more direct comparison between  
 557 the simulations and observations. Specifically, the SOC mass concentration ( $C_{SOC}$ ) is related to the  
 558 SOA mass concentration ( $C_{SOA}$ ) for a given SOA type through the relationship:

$$559 \quad C_{SOC} = C_{SOA} \cdot \frac{N_C \cdot MW_C}{MW_{SOA}} = \frac{N_C \cdot MW_C}{N_C \cdot MW_C + N_O \cdot MW_O + N_H \cdot MW_H} = \frac{C_{SOA}}{\frac{4}{3}(O:C) + \frac{1}{12}(H:C) + 1} \quad (4)$$

560 where  $MW_C$ ,  $MW_O$ ,  $MW_H$  are the molecular weights of carbon, oxygen and hydrogen atoms,  
 561 respectively. The O:C and H:C values of the different SOA types are not constant in the SOM due  
 562 to the continuous evolution of the product distribution. However, for a given SOA type the  
 563 simulated O:C and H:C values vary over a relatively narrow range (Cappa et al., 2013) and thus  
 564 an average value can be used. The resulting  $F_{SOC, fossil}$  values are compared with the  $F_{SOA, fossil}$  values  
 565 in Table S2 and are found to be very similar. The  $F_{OOC, fossil}$  values were determined from  $^{14}C$   
 566 analysis of particles collected on filters to allow determination of the fossil fraction of the total  
 567 carbonaceous material coupled with positive matrix factorization to allow separation of the  
 568 contributions from the various fossil and non-fossil POA and SOA sources. The uncertainty in the  
 569 fossil fraction of total OC was reported as 9%; the uncertainty in the  $F_{OOC, fossil}$  will be larger. Zotter  
 570 et al. (2014) determined the nighttime  $F_{OOC, fossil}$  was smaller than the peak daytime value and that  
 571 the 24-h average best-estimate  $F_{OOC, fossil} = 44\%$ . This is somewhat larger than the average predicted  
 572  $F_{SOC, fossil}$  (e.g. 31% for SOM-high). The difference between the observed  $F_{OOC, fossil}$  and predicted  
 573  $F_{SOC, fossil}$  could indicate a role for SOA formed from fossil-derived S/IVOC species in the  
 574 atmosphere but which are not considered here.

### 575 4.3.2 The Oxygen-to-Carbon Ratio

576 The O:C atomic ratios of the SOA have been calculated from the simulated distributions of  
 577 compounds in  $N_C$  and  $N_O$  space; the O:C atomic ratio is an inherent property of the SOM model  
 578 and  $(O:C)_{SOA}$  values from box model simulations using SOM exhibit generally good agreement  
 579 with observations (Cappa and Wilson, 2012; Cappa et al., 2013). Few air quality models attempt

580 to simulate O:C ratios for SOA (e.g. Murphy et al., 2011), although a dramatic expansion in  
581 observations of O:C ratios for ambient OA has recently occurred (Ng et al., 2011; Canagaratna et  
582 al., 2015; Chen et al., 2015). Comparison between intensive properties such as O:C, in addition to  
583 absolute OA concentrations, can provide further constraints on the transformation processes and  
584 OA sources in a given region. The simulated  $(\text{O:C})_{\text{SOA}}$  in the SOM-no simulations are generally  
585 larger in SoCAB than in the eastern US (Figure 6). The simulated  $(\text{O:C})_{\text{SOA}}$  from isoprene and  
586 aromatics individually are larger than those from mono- or sesquiterpenes due, in large part, to the  
587 smaller carbon backbone and the need to add more oxygens to produce sufficiently low volatility  
588 species that partition substantially to the particle phase (Chhabra et al., 2011; Cappa and Wilson,  
589 2012; Tkacik et al., 2012). Thus, the larger  $(\text{O:C})_{\text{SOA}}$  in SoCAB results from larger relative  
590 contributions from isoprene and aromatic compounds to the total SOA burden in this region. The  
591  $(\text{O:C})_{\text{SOA}}$  is also generally larger in regions where SOA concentrations are smaller. This may  
592 reflect some relationship between SOA source and concentration, but it also reflects the role that  
593 continued multi-generational oxidation has on the SOA composition, since lower concentrations  
594 can reflect greater dilution and overall more aged SOA.

595 The  $(\text{O:C})_{\text{SOA}}$  for the SOM-low and SOM-high simulations are substantially larger than that  
596 from the SOM-no simulations in both SoCAB and the eastern US (Figure 6). This reflects two  
597 phenomena: (i) the increased relative contribution of isoprene to the total simulated SOA burden  
598 in the SOM-low and SOM-high simulations and (ii) differences in the SOM chemical pathways  
599 (i.e. the SOM parameters) that lead to the production of condensed-phase material between the  
600 parameterizations that do/do not include vapor wall losses. The influence of the latter has been  
601 confirmed through box model simulations, although the exact behavior is both precursor specific  
602 and somewhat dependent on the reaction conditions (e.g.  $[\text{OH}]$  and the initial precursor  
603 concentration). Overall, the former effect likely dominates since the difference in simulated  
604  $(\text{O:C})_{\text{SOA}}$  between isoprene and monoterpenes is substantial (Jathar et al., 2015a).

605 The simulated O:C for the total OA also differs substantially between simulations (Figure 7),  
606 especially in regions where the simulated increase in  $f_{\text{SOA}}$  is largest (Figure 2). The simulated  
607  $(\text{O:C})_{\text{total}}$  in both the SoCAB and eastern US increases substantially when vapor wall losses are  
608 accounted for. For example, the simulated  $(\text{O:C})_{\text{total}}$  values at Riverside were 0.22, 0.3 and 0.42  
609 and at Atlanta were 0.45, 0.65 and 0.85 for SOM-no, SOM-low and SOM-high simulations,  
610 respectively. The increase in  $(\text{O:C})_{\text{total}}$  is mostly driven by an associated increase in  $f_{\text{SOA}}$ . The

611 (O:C)<sub>total</sub> value is a weighted average of the (O:C)<sub>SOA</sub> and (O:C)<sub>POA</sub>, with  $(O:C)_{total} = (n_{O,SOA} +$   
612  $n_{O,POA}) / (n_{C,SOA} + n_{C,POA})$  where  $n_O$  and  $n_C$  indicate the number of oxygen and carbon atoms,  
613 respectively, that comprise all SOA types and POA. For conceptual purposes, this exact expression  
614 for (O:C)<sub>total</sub> can be approximated as  $(O:C)_{total} \sim f_{SOA}(O:C)_{SOA} + (1-f_{SOA})(O:C)_{POA}$ , where (O:C)<sub>SOA</sub>  
615 represents the average over the different SOA types. Thus, changes in  $f_{SOA}$  lead to changes in  
616 (O:C)<sub>total</sub>, with some additional smaller changes due to variation in the weighted average (O:C)<sub>SOA</sub>  
617 between the various simulations (since each SOA type has a particular O:C range). The predicted  
618 eastern US (O:C)<sub>total</sub> are generally larger than in SoCAB due to the larger  $f_{SOA}$  in the eastern US  
619 and since (O:C)<sub>SOA</sub> is typically larger than (O:C)<sub>POA</sub>. For example, the average (O:C)<sub>total</sub> in Atlanta  
620 for the SOM-no simulations was 0.4 whereas it was 0.22 in Riverside.

621 The simulated results at Riverside can be compared with bulk, campaign average (O:C)<sub>total</sub>  
622 values measured during the SOAR campaign using an Aerodyne high resolution time-of-flight  
623 aerosol mass spectrometer (HR-AMS), which determines (O:C)<sub>total</sub> with an absolute uncertainty of  
624  $\pm 30\%$  but with very high precision (Docherty et al., 2008; Dzepina et al., 2009). Values reported  
625 here have been corrected according to Canagaratna et al. (2015). The campaign-average observed  
626 (O:C)<sub>total</sub> was  $\sim 0.45$ . The SOM-high (O:C)<sub>total</sub> is in very good agreement with the observations,  
627 whereas (O:C)<sub>total</sub> is too small for both SOM-no and SOM-low. This good correspondence is, of  
628 course, sensitive to the assumed (O:C)<sub>POA</sub>, here 0.2 based on (Ng et al., 2011). If a smaller (O:C)<sub>POA</sub>  
629 had been assumed, then either a greater amount of SOA would be required or the simulated  
630 (O:C)<sub>SOA</sub> would need to be larger to match the SOAR measurements. Docherty et al. (2011)  
631 determined there were three POA types during SOAR, with a weighted-average corrected O:C =  
632 0.095, suggesting that the assumed 0.2 is too large. In contrast, Hayes et al. (2013) determined a  
633 weighted-average corrected O:C = 0.25 for the three POA types identified at Pasadena during  
634 CalNex. It has been suggested that at least some of the difference in the (O:C)<sub>POA</sub> between SOAR  
635 and CalNex results from greater heterogeneous ageing of the Pasadena POA. Regardless of the  
636 exact (O:C)<sub>POA</sub>, a strong improvement in the model-measurement agreement when vapor wall  
637 losses are accounted for is evident. Of additional consideration is the diurnal dependence of the  
638 (O:C)<sub>total</sub>. The observed (O:C)<sub>total</sub> exhibited a distinct diurnal dependence, with low values at night,  
639 a minimum at  $\sim 7$  am and maximum values around midday (Figure 8). The simulated (O:C)<sub>total</sub>  
640 diurnal profile for the SOM-high simulations agrees reasonably well with the SOAR observations  
641 in terms of both the magnitude of the day-night difference and the absolute (O:C)<sub>total</sub> (Figure 8). In

642 contrast, both the SOM-no and SOM-low exhibit only minor variations with time-of-day due to  
643 the controlling influence of  $(\text{O:C})_{\text{POA}}$ .

644 The simulated  $(\text{O:C})_{\text{total}}$  values in the eastern US can also be compared with recent  
645 observations, with the caveat that in this case the measurements were not made over the same time-  
646 period as the simulations were run. Nonetheless, measurements made in summer and winter of  
647 2012 and 2013 at various locations in Alabama and Georgia indicate the O:C values for total OA  
648 were relatively constant, around 0.6-0.7, although it should be noted that these values were  
649 estimated from measurements made using an Aerodyne aerosol chemical speciation monitor,  
650 which increases the uncertainty (Xu et al., 2015b). Measurements made around the southeast US  
651 using an HR-AMS onboard the NASA DC8 as part of the SEAC4RS field study indicate the  
652 average  $(\text{O:C})_{\text{total}} = 0.8$  when the plane was flying below 1 km (SEAC4RS). As noted above, the  
653 simulated  $(\text{O:C})_{\text{total}}$  around Atlanta was 0.45 for SOM-no, increasing to  $\sim 0.65$  for SOM-low and  
654  $\sim 0.85$  for SOM-high. As with the SoCAB comparison, the general level of agreement between the  
655 observed and simulated  $(\text{O:C})_{\text{tot}}$  was improved when vapor wall losses were accounted for.

656 The above simulations included SOA only from VOCs, neglecting contributions from  
657 S/IVOCs including oxidation of semi-volatile POA vapors. S/IVOCs and semi-volatile POA  
658 vapors are likely  $\geq \text{C}_{14}$  carbon species (Jathar et al., 2014; Zhao et al., 2014). As such, little added oxygen  
659 is required to produce low-volatility species that will form SOA. Since these species also have  
660 relatively large number of carbon atoms, the O:C of the SOA formed from them will be relatively  
661 small, most likely with  $(\text{O:C})_{\text{S/IVOC}} < 0.2$  in the absence of strong heterogeneous oxidation (Cappa  
662 and Wilson, 2012; Tkacik et al., 2012); note that this range is lower than what was assumed for  
663 the non-volatile POA here. Consequently, had S/IVOCs been included in the simulations the  
664  $(\text{O:C})_{\text{total}}$  would have likely decreased. The magnitude of the decrease would depend on the exact  
665 extent to which the S/IVOCs contributed to the overall SOA burden, the extent to which the  
666 simulated POA decreased (due to the semi-volatile treatment), and on the simulated  $(\text{O:C})_{\text{S/IVOC}}$ .  
667 In the limit that SOA from S/IVOCs dominates the SOA budget, very little variation in the  
668  $(\text{O:C})_{\text{total}}$  ratio with time of day would have likely been predicted because  $(\text{O:C})_{\text{POA}} \sim (\text{O:C})_{\text{S/IVOC}}$ .  
669 Additionally, the simulated daytime  $(\text{O:C})_{\text{total}}$  values would have likely been close to 0.2. A lack  
670 of diurnal variability and a small  $(\text{O:C})_{\text{total}}$  would both be inconsistent with the SOAR observations.  
671 Consequently, this implies that accounting for vapor wall losses has a stronger potential to allow  
672 for simultaneous reconciliation of the diurnal behavior of both the simulated OA/ $\Delta\text{CO}$  and

673 (O:C)<sub>total</sub> with observations than does consideration of oxidation of S/IVOCs alone. This is not to  
674 say that S/IVOC contributions to the SOA and total OA burden are not important, only that it  
675 seems unlikely that they could dominate the SOA budget. Ultimately, it seems likely that  
676 consideration of both vapor wall losses (as done here) and of SOA from S/IVOCs will be necessary  
677 to fully close the model/measurement gap.

678

## 679 **5 Conclusions**

680 The influence of chamber vapor wall losses on simulated SOA concentrations and properties  
681 has been assessed. The statistical oxidation model was used to parameterize SOA formation from  
682 laboratory chamber experiments both with and without accounting for vapor wall losses using data  
683 from experiments conducted under both high-NO<sub>x</sub> and low-NO<sub>x</sub> conditions. “Low” and a “high”  
684 vapor wall loss cases were considered in addition to the “no” vapor wall loss case. The best-fit  
685 SOM parameters under these different conditions were used as input to SOA simulations in the  
686 3D UCD/CIT regional air quality model, in which SOM has been recently implemented (Jathar et  
687 al., 2015a). Simulations were run for southern California and for the eastern US. Explicit  
688 accounting for vapor wall losses led to increases in simulated SOA concentrations, by a factor of  
689 ~2-5 for the “low” simulations and ~5-10 for the “high” simulations. The magnitude of the increase  
690 was inversely related to the simulated absolute SOA concentration. This suggests that the extent  
691 to which SOA concentrations are underpredicted may be greater in more remote regions.

692 This increase in simulated SOA when vapor wall losses are accounted for leads to a substantial  
693 increase in the simulated SOA fraction of total OA. This is especially seen in SoCAB where  $f_{\text{SOA}}$   
694 is very small for the base model but >50% for the simulations that account for vapor wall losses.  
695 The simulated  $f_{\text{SOA}}$  in SoCAB is found to agree reasonably well with observations when vapor wall  
696 losses are accounted for. Comparison of the OA/ $\Delta$ CO from the SoCAB simulations with  
697 observations from the SOAR campaign (Docherty et al., 2008) indicate that accounting for vapor  
698 wall losses leads to substantially improved agreement in terms of the diurnal behavior, in particular  
699 the magnitude of the daytime increase in OA/ $\Delta$ CO. Accounting for vapor wall losses also leads to  
700 location-specific changes in the major contributing VOC precursors to the SOA burden. In general,  
701 accounting for vapor wall losses leads to an increase in the predicted relative contribution of  
702 isoprene SOA and a decrease in the relative contribution of monoterpene and sesquiterpene SOA.

703 The relative contribution of total anthropogenic VOCs to SOA is reasonably insensitive to vapor  
704 wall losses, especially in SoCAB, although the apportionment between aromatic VOCs and  
705 alkanes does vary with vapor wall losses. The simulated anthropogenic SOA fraction is, however,  
706 somewhat smaller than suggested by <sup>14</sup>C observations during CalNex (Zotter et al., 2014). In  
707 general, the simulated O:C atomic ratio of the SOA increased for the low and high vapor wall loss  
708 simulations, compared to the base case. The simulated O:C of the total OA (SOA + POA) in both  
709 SoCAB and the eastern US are in better agreement with observations when vapor wall losses are  
710 accounted for.

711 Overall, the generally improved model performance when vapor wall losses are accounted  
712 for—in terms of both absolute and relative concentrations and in terms of SOA properties—  
713 suggests that accounting for this chamber effect in atmospheric simulations of SOA is important,  
714 although certainly requiring further examination. Our results qualitatively agree with other recent  
715 efforts to assess the influence of vapor wall losses on ambient SOA concentrations (Baker et al.,  
716 2015; Hayes et al., 2015), but as our accounting for vapor wall loss is inherent in the SOA  
717 parameterization the simulations here serve to provide a more robust assessment. The results  
718 presented here additionally suggest that there may be no need to invoke *ad hoc* “ageing” schemes  
719 for aromatics (Tsimpidi et al., 2010) to achieve increases in simulated SOA concentrations in urban  
720 environments. Further, these results suggest that that the contribution of S/IVOCs to urban SOA  
721 might be somewhat limited, albeit still important, although this issue certainly requires further  
722 investigation.

723

## 724 **Author Contributions**

725 The manuscript was written through contributions of all authors. CDC, SHJ, MJK, JHS and  
726 ASW designed the project. SHJ and MJK carried out the simulations. CDC determined model  
727 parameters using laboratory data collected by JHS. KSD and JLJ collected and processed the  
728 SOAR data. All authors have given approval to the final version of the manuscript.

729

## 730 **Acknowledgements**

731 The authors thank Pedro Campuzano-Jost for the SEAC4RS data. This study was funded by the  
732 California Air Resources Board, contract 12-312 and NOAA grant NA13OAR4310058. JLJ was  
733 supported by CARB 11-305 and EPA STAR 83587701-0. This manuscript has not been reviewed  
734 by the funding agencies and no endorsement should be inferred.

735

## 736 **References**

737 Baker, K. R., Carlton, A. G., Kleindienst, T. E., Offenberg, J. H., Beaver, M. R., Gentner, D. R.,  
738 Goldstein, A. H., Hayes, P. L., Jimenez, J. L., Gilman, J. B., de Gouw, J. A., Woody, M. C., Pye,  
739 H. O. T., Kelly, J. T., Lewandowski, M., Jaoui, M., Stevens, P. S., Brune, W. H., Lin, Y. H.,  
740 Rubitschun, C. L., and Surratt, J. D.: Gas and aerosol carbon in California: comparison of  
741 measurements and model predictions in Pasadena and Bakersfield, *Atmos. Chem. Phys.*, 15,  
742 5243-5258, doi:10.5194/acp-15-5243-2015, 2015.

743 Budisulistiorini, S. H., Canagaratna, M. R., Croteau, P. L., Marth, W. J., Baumann, K., Edgerton,  
744 E. S., Shaw, S. L., Knipping, E. M., Worsnop, D. R., Jayne, J. T., Gold, A., and Surratt, J. D.:  
745 Real-Time Continuous Characterization of Secondary Organic Aerosol Derived from Isoprene  
746 Epoxydiols in Downtown Atlanta, Georgia, Using the Aerodyne Aerosol Chemical Speciation  
747 Monitor, *Environ. Sci. Technol.*, 47, 5686-5694, doi:10.1021/es400023n, 2013.

748 Canagaratna, M. R., Jimenez, J. L., Kroll, J. H., Chen, Q., Kessler, S. H., Massoli, P.,  
749 Hildebrandt Ruiz, L., Fortner, E., Williams, L. R., Wilson, K. R., Surratt, J. D., Donahue, N. M.,  
750 Jayne, J. T., and Worsnop, D. R.: Elemental ratio measurements of organic compounds using  
751 aerosol mass spectrometry: characterization, improved calibration, and implications, *Atmos.*  
752 *Chem. Phys.*, 15, 253-272, doi:10.5194/acp-15-253-2015, 2015.

753 Cappa, C. D. and Wilson, K. R.: Multi-generation gas-phase oxidation, equilibrium partitioning,  
754 and the formation and evolution of secondary organic aerosol, *Atmos. Chem. Phys.*, 12, 9505-  
755 9528, doi:10.5194/acp-12-9505-2012, 2012.

756 Cappa, C. D., Zhang, X., Loza, C. L., Craven, J. S., Yee, L. D., and Seinfeld, J. H.: Application  
757 of the Statistical Oxidation Model (SOM) to secondary organic aerosol formation from  
758 photooxidation of C12 Alkanes, *Atmos. Chem. Phys.*, 13, 1591-1606, doi:10.5194/acp-13-1591-  
759 2013, 2013.

760 Carlton, A. G., Bhave, P. V., Napelenok, S. L., Edney, E. O., Sarwar, G., Pinder, R. W., Pouliot,  
761 G. A., and Houyoux, M.: Model Representation of Secondary Organic Aerosol in CMAQv4.7,  
762 *Environ. Sci. Technol.*, 44, 8553-8560, doi:10.1021/es100636q, 2010.

763 Chen, Q., Heald, C. L., Jimenez, J. L., Canagaratna, M. R., Qi, Z., Ling-Yan, H., Xiao-Feng, H.,  
764 Campuzano-Jost, P., Palm, B. B., Poulain, L., Kuwata, M., Martin, S. T., Abbatt, J. P. D., Lee,  
765 A. K. Y., and Liggi, J.: Elemental composition of organic aerosol: the gap between ambient and  
766 laboratory measurements, *Geophys. Res. Lett.*, 42, 4182-4189, doi:10.1002/2015gl063693, 2015.

767 Chhabra, P. S., Ng, N. L., Canagaratna, M. R., Corrigan, A. L., Russell, L. M., Worsnop, D. R.,  
768 Flagan, R. C., and Seinfeld, J. H.: Elemental composition and oxidation of chamber organic  
769 aerosol, *Atmos. Chem. Phys.*, 11, 8827-8845, doi:10.5194/acp-11-8827-2011, 2011.

770 De Gouw, J. and Jimenez, J. L.: Organic Aerosols in the Earth's Atmosphere, *Environ. Sci.*  
771 *Technol.*, 43, 7614-7618, doi:10.1021/es9006004, 2009.

772 Docherty, K. S., Aiken, A. C., Huffman, J. A., Ulbrich, I. M., DeCarlo, P. F., Sueper, D.,  
773 Worsnop, D. R., Snyder, D. C., Peltier, R. E., Weber, R. J., Grover, B. D., Eatough, D. J.,  
774 Williams, B. J., Goldstein, A. H., Ziemann, P. J., and Jimenez, J. L.: The 2005 Study of Organic  
775 Aerosols at Riverside (SOAR-1): instrumental intercomparisons and fine particle composition,  
776 *Atmos. Chem. Phys.*, 11, 12387-12420, doi:10.5194/acp-11-12387-2011, 2011.

777 Docherty, K. S., Stone, E. A., Ulbrich, I. M., DeCarlo, P. F., Snyder, D. C., Schauer, J. J., Peltier,  
778 R. E., Weber, R. J., Murphy, S. M., Seinfeld, J. H., Grover, B. D., Eatough, D. J., and Jimenez, J.  
779 L.: Apportionment of Primary and Secondary Organic Aerosols in Southern California during  
780 the 2005 Study of Organic Aerosols in Riverside (SOAR-1), *Environ. Sci. Technol.*, 42, 7655-  
781 7662, doi:10.1021/es8008166, 2008.

782 Dzepina, K., Cappa, C. D., Volkamer, R. M., Madronich, S., DeCarlo, P. F., Zaveri, R. A., and  
783 Jimenez, J. L.: Modeling the Multiday Evolution and Aging of Secondary Organic Aerosol  
784 During MILAGRO 2006, *Environ. Sci. Technol.*, 45, 3496-3503, doi:10.1021/es103186f, 2011.

785 Dzepina, K., Volkamer, R. M., Madronich, S., Tulet, P., Ulbrich, I. M., Zhang, Q., Cappa, C. D.,  
786 Ziemann, P. J., and Jimenez, J. L.: Evaluation of recently-proposed secondary organic aerosol  
787 models for a case study in Mexico City, *Atmos. Chem. Phys.*, 9, 5681-5709, doi:10.5194/acp-9-  
788 5681-2009, 2009.

789 Ensberg, J. J., Hayes, P. L., Jimenez, J. L., Gilman, J. B., Kuster, W. C., de Gouw, J. A.,  
790 Holloway, J. S., Gordon, T. D., Jathar, S. H., Robinson, A. L., and Seinfeld, J. H.: Emission  
791 factor ratios, SOA mass yields, and the impact of vehicular emissions on SOA formation, *Atmos.*  
792 *Chem. Phys.*, 14, 2383-2397, doi:10.5194/acp-14-2383-2014, 2013.

793 Ervens, B., Turpin, B. J., and Weber, R. J.: Secondary organic aerosol formation in cloud  
794 droplets and aqueous particles (aqSOA): a review of laboratory, field and model studies, *Atmos.*  
795 *Chem. Phys.*, 11, 11069-11102, doi:10.5194/acp-11-11069-2011, 2011.

796 Hayes, P. L., Carlton, A. G., Baker, K. R., Ahmadov, R., Washenfelder, R. A., Alvarez, S.,  
797 Rappenglück, B., Gilman, J. B., Kuster, W. C., de Gouw, J. A., Zotter, P., Prévôt, A. S. H.,  
798 Szidat, S., Kleindienst, T. E., Offenberg, J. H., and Jimenez, J. L.: Modeling the formation and  
799 aging of secondary organic aerosols in Los Angeles during CalNex 2010, *Atmos. Chem. Phys.*,  
800 15, 5773-5801, doi:10.5194/acp-15-5773-2015, 2015.

801 Hayes, P. L., Ortega, A. M., Cubison, M. J., Froyd, K. D., Zhao, Y., Cliff, S. S., Hu, W. W.,  
802 Toohey, D. W., Flynn, J. H., Lefer, B. L., Grossberg, N., Alvarez, S., Rappenglück, B., Taylor, J.  
803 W., Allan, J. D., Holloway, J. S., Gilman, J. B., Kuster, W. C., de Gouw, J. A., Massoli, P.,  
804 Zhang, X., Liu, J., Weber, R. J., Corrigan, A. L., Russell, L. M., Isaacman, G., Worton, D. R.,  
805 Kreisberg, N. M., Goldstein, A. H., Thalman, R., Waxman, E. M., Volkamer, R., Lin, Y. H.,  
806 Surratt, J. D., Kleindienst, T. E., Offenberg, J. H., Dusanter, S., Griffith, S., Stevens, P. S.,  
807 Brioude, J., Angevine, W. M., and Jimenez, J. L.: Organic aerosol composition and sources in  
808 Pasadena, California, during the 2010 CalNex campaign, *J. Geophys. Res.-Atmos.*, 118, 9233-  
809 9257, doi:10.1002/jgrd.50530, 2013.

810 Heald, C. L., Jacob, D. J., Park, R. J., Russell, L. M., Huebert, B. J., Seinfeld, J. H., Liao, H., and  
811 Weber, R. J.: A large organic aerosol source in the free troposphere missing from current  
812 models, *Geophys. Res. Lett.*, 32, L18809, doi:10.1029/2005GL023831, 2005.

813 Hodzic, A., Aumont, B., Knote, C., Lee-Taylor, J., Madronich, S., and Tyndall, G.: Volatility  
814 dependence of Henry's law constants of condensable organics: Application to estimate  
815 depositional loss of secondary organic aerosols, *Geophys. Res. Lett.*, 41, 4795-4804,  
816 doi:10.1002/2014gl060649, 2014.

817 Hodzic, A., Kasibhatla, P. S., Jo, D. S., Cappa, C. D., Jimenez, J. L., Madronich, S., and Park, R.  
818 J.: Rethinking the global secondary organic aerosol (SOA) budget: stronger production, faster  
819 removal, shorter lifetime, *Atmos. Chem. Phys. Discuss.*, 15, 32413-32468, doi:10.5194/acpd-15-  
820 32413-2015, 2015.

821 Hu, W. W., Campuzano-Jost, P., Palm, B. B., Day, D. A., Ortega, A. M., Hayes, P. L.,  
822 Krechmer, J. E., Chen, Q., Kuwata, M., Liu, Y. J., de Sá, S. S., Martin, S. T., Hu, M.,  
823 Budisulistiorini, S. H., Riva, M., Surratt, J. D., St. Clair, J. M., Isaacman-Van Wertz, G., Yee, L.  
824 D., Goldstein, A. H., Carbone, S., Artaxo, P., de Gouw, J. A., Koss, A., Wisthaler, A., Mikoviny,  
825 T., Karl, T., Kaser, L., Jud, W., Hansel, A., Docherty, K. S., Robinson, N. H., Coe, H., Allan, J.  
826 D., Canagaratna, M. R., Paulot, F., and Jimenez, J. L.: Characterization of a real-time tracer for  
827 Isoprene Epoxydiols-derived Secondary Organic Aerosol (IEPOX-SOA) from aerosol mass  
828 spectrometer measurements, *Atmos. Chem. Phys.*, 15, 11807-11833, doi:10.5194/acp-15-11807-  
829 2015, 2015.

830 Jathar, S. H., Cappa, C. D., Wexler, A. S., Seinfeld, J. H., and Kleeman, M. J.: Multi-  
831 generational Oxidation Model to Simulate Secondary Organic Aerosol in a 3D Air Quality  
832 Model, *Geosci. Model Dev.*, 8, 2553-2567, doi:10.5194/gmd-8-2553-2015, 2015a.

833 Jathar, S. H., Cappa, C. D., Wexler, A. S., Seinfeld, J. H., and Kleeman, M. J.: Simulating  
834 secondary organic aerosol in a regional air quality model using the statistical oxidation model –  
835 Part 1: Assessing the influence of constrained multi-generational ageing, *Atmos. Chem. Phys.*  
836 *Discuss.*, 15, 25837-25872, doi:10.5194/acpd-15-25837-2015, 2015b.

837 Jathar, S. H., Gordon, T. D., Hennigan, C. J., Pye, H. O. T., Pouliot, G., Adams, P. J., Donahue,  
838 N. M., and Robinson, A. L.: Unspeciated organic emissions from combustion sources and their  
839 influence on the secondary organic aerosol budget in the United States, *Proc. Nat. Acad. Sci.*,  
840 111, 10473-10478, doi:10.1073/pnas.1323740111, 2014.

841 Kim, P. S., Jacob, D. J., Fisher, J. A., Travis, K., Yu, K., Zhu, L., Yantosca, R. M., Sulprizio, M.  
842 P., Jimenez, J. L., Campuzano-Jost, P., Froyd, K. D., Liao, J., Hair, J. W., Fenn, M. A., Butler, C.  
843 F., Wagner, N. L., Gordon, T. D., Welti, A., Wennberg, P. O., Crounse, J. D., St. Clair, J. M.,  
844 Teng, A. P., Millet, D. B., Schwarz, J. P., Markovic, M. Z., and Perring, A. E.: Sources,  
845 seasonality, and trends of southeast US aerosol: an integrated analysis of surface, aircraft, and  
846 satellite observations with the GEOS-Chem chemical transport model, *Atmos. Chem. Phys.*, 15,  
847 10411-10433, doi:10.5194/acp-15-10411-2015, 2015.

848 Kleeman, M. J. and Cass, G. R.: A 3D Eulerian Source-Oriented Model for an Externally Mixed  
849 Aerosol, *Environ. Sci. Technol.*, 35, 4834-4848, doi:10.1021/es010886m, 2001.

850 Kokkola, H., Yli-Pirilä, P., Vestnerinen, M., Korhonen, H., Keskinen, H., Romakkaniemi, S.,  
851 Hao, L., Kortelainen, A., Joutsensaari, J., Worsnop, D. R., Virtanen, A., and Lehtinen, K. E. J.:  
852 The role of low volatile organics on secondary organic aerosol formation, *Atmos. Chem. Phys.*,  
853 14, 1689-1700, doi:10.5194/acp-14-1689-2014, 2014.

854 Krechmer, J. E., Coggon, M. M., Massoli, P., Nguyen, T. B., Crounse, J. D., Hu, W., Day, D. A.,  
855 Tyndall, G. S., Henze, D. K., Rivera-Rios, J. C., Nowak, J. B., Kimmel, J. R., Mauldin, R. L.,

856 Stark, H., Jayne, J. T., Sipilä, M., Junninen, H., Clair, J. M. S., Zhang, X., Feiner, P. A., Zhang,  
857 L., Miller, D. O., Brune, W. H., Keutsch, F. N., Wennberg, P. O., Seinfeld, J. H., Worsnop, D.  
858 R., Jimenez, J. L., and Canagaratna, M. R.: Formation of Low Volatility Organic Compounds  
859 and Secondary Organic Aerosol from Isoprene Hydroxyhydroperoxide Low-NO Oxidation,  
860 *Environ. Sci. Technol.*, 49, 10330-10339, doi:10.1021/acs.est.5b02031, 2015.

861 Lane, T. E., Donahue, N. M., and Pandis, S. N.: Effect of NO<sub>x</sub> on Secondary Organic Aerosol  
862 Concentrations, *Environ. Sci. Technol.*, 42, 6022-6027, doi:10.1021/es703225a, 2008a.

863 Lane, T. E., Donahue, N. M., and Pandis, S. N.: Simulating secondary organic aerosol formation  
864 using the volatility basis-set approach in a chemical transport model, *Atmos. Environ.*, 42, 7439-  
865 7451, doi:10.1016/j.atmosenv.2008.06.026, 2008b.

866 Matsunaga, A. and Ziemann, P. J.: Gas-Wall Partitioning of Organic Compounds in a Teflon  
867 Film Chamber and Potential Effects on Reaction Product and Aerosol Yield Measurements,  
868 *Aerosol Sci. Technol.*, 44, 881-892, doi:10.1080/02786826.2010.501044, 2010.

869 McVay, R. C., Cappa, C. D., and Seinfeld, J. H.: Vapor–Wall Deposition in Chambers:  
870 Theoretical Considerations, *Environ. Sci. Technol.*, 48, 10251-10258, doi:10.1021/es502170j,  
871 2014.

872 Murphy, B. N., Donahue, N. M., Fountoukis, C., and Pandis, S. N.: Simulating the oxygen  
873 content of ambient organic aerosol with the 2D volatility basis set, *Atmos. Chem. Phys.*, 11,  
874 7859-7873, doi:10.5194/acp-11-7859-2011, 2011.

875 Ng, N. L., Canagaratna, M. R., Jimenez, J. L., Chhabra, P. S., Seinfeld, J. H., and Worsnop, D.  
876 R.: Changes in organic aerosol composition with aging inferred from aerosol mass spectra,  
877 *Atmos. Chem. Phys.*, 11, 6465-6474, doi:10.5194/acp-11-6465-2011, 2011.

878 Ng, N. L., Chhabra, P. S., Chan, A. W. H., Surratt, J. D., Kroll, J. H., Kwan, A. J., McCabe, D.  
879 C., Wennberg, P. O., Sorooshian, A., Murphy, S. M., Dalleska, N. F., Flagan, R. C., and  
880 Seinfeld, J. H.: Effect of NO<sub>x</sub> level on secondary organic aerosol (SOA) formation from the  
881 photooxidation of terpenes, *Atmos. Chem. Phys.*, 7, 5159-5174, doi:10.5194/acp-7-5159-2007,  
882 2007a.

883 Ng, N. L., Kroll, J. H., Chan, A. W. H., Chhabra, P. S., Flagan, R. C., and Seinfeld, J. H.:  
884 Secondary organic aerosol formation from m-xylene, toluene, and benzene, *Atmos. Chem. Phys.*,  
885 7, 3909-3922, doi:10.5194/acp-7-3909-2007, 2007b.

886 Odum, J. R., Hoffmann, T., Bowman, F., Collins, D., Flagan, R. C., and Seinfeld, J. H.:  
887 Gas/particle partitioning and secondary organic aerosol yields, *Environ. Sci. Technol.*, 30, 2580-  
888 2585, doi:10.1021/es950943+, 1996.

889 Pankow, J. F.: An absorption-model of the gas aerosol partitioning involved in the formation of  
890 secondary organic aerosol, *Atmos. Environ.*, 28, 189-193, doi:10.1016/1352-2310(94)90094-9,  
891 1994.

892 Pye, H. O. T., Pinder, R. W., Piletic, I. R., Xie, Y., Capps, S. L., Lin, Y.-H., Surratt, J. D., Zhang,  
893 Z., Gold, A., Luecken, D. J., Hutzell, W. T., Jaoui, M., Offenberg, J. H., Kleindienst, T. E.,  
894 Lewandowski, M., and Edney, E. O.: Epoxide Pathways Improve Model Predictions of Isoprene  
895 Markers and Reveal Key Role of Acidity in Aerosol Formation, *Environ. Sci. Technol.*, 47,  
896 11056-11064, doi:10.1021/es402106h, 2013.

897 Robinson, A. L., Donahue, N. M., Shrivastava, M. K., Weitkamp, E. A., Sage, A. M., Grieshop,  
898 A. P., Lane, T. E., Pierce, J. R., and Pandis, S. N.: Rethinking organic aerosols: Semivolatile  
899 emissions and photochemical aging, *Science*, 315, 1259-1262, doi:10.1126/science.1133061,  
900 2007.

901 Russell, A. R., Valin, L. C., and Cohen, R. C.: Trends in OMI NO<sub>2</sub> observations over the United  
902 States: effects of emission control technology and the economic recession, *Atmos. Chem. Phys.*,  
903 12, 12197-12209, doi:10.5194/acp-12-12197-2012, 2012.

904 SEAC4RS: Studies of Emissions and Atmospheric Composition, Clouds and Climate Coupling  
905 by Regional Surveys, doi: 10.5067/Aircraft/SEAC4RS/Aerosol-TraceGas-Cloud, NASA  
906 Langley Research Center, Hampton, VA, USA, 2014.

907 Simon, H. and Bhawe, P. V.: Simulating the Degree of Oxidation in Atmospheric Organic  
908 Particles, *Environ. Sci. Technol.*, 46, 331-339, doi:10.1021/es202361w, 2011.

909 Subramanian, R., Khlystov, A. Y., Cabada, J. C., and Robinson, A. L.: Positive and Negative  
910 Artifacts in Particulate Organic Carbon Measurements with Denuded and Undenuded Sampler  
911 Configurations, *Aerosol Sci. Technol.*, 38, 27-48, doi:10.1080/02786820390229354, 2004.

912 The Visibility Information Exchange Web System (VIEWS 2.0): The Visibility Information  
913 Exchange Web System, <http://views.cira.colostate.edu/web/>, Colorado State University, last  
914 access: 11 February 2015, 2015.

915 Tkacik, D. S., Presto, A. A., Donahue, N. M., and Robinson, A. L.: Secondary Organic Aerosol  
916 Formation from Intermediate-Volatility Organic Compounds: Cyclic, Linear, and Branched  
917 Alkanes, *Environ. Sci. Technol.*, 46, 8773-8781, doi:10.1021/es301112c, 2012.

918 Tsigaridis, K., Daskalakis, N., Kanakidou, M., Adams, P. J., Artaxo, P., Bahadur, R., Balkanski,  
919 Y., Bauer, S. E., Bellouin, N., Benedetti, A., Bergman, T., Berntsen, T. K., Beukes, J. P., Bian,  
920 H., Carslaw, K. S., Chin, M., Curci, G., Diehl, T., Easter, R. C., Ghan, S. J., Gong, S. L., Hodzic,  
921 A., Hoyle, C. R., Iversen, T., Jathar, S., Jimenez, J. L., Kaiser, J. W., Kirkevåg, A., Koch, D.,  
922 Kokkola, H., Lee, Y. H., Lin, G., Liu, X., Luo, G., Ma, X., Mann, G. W., Mihalopoulos, N.,  
923 Morcrette, J. J., Müller, J. F., Myhre, G., Myriokefalitakis, S., Ng, N. L., O'Donnell, D., Penner,  
924 J. E., Pozzoli, L., Pringle, K. J., Russell, L. M., Schulz, M., Sciare, J., Seland, Ø., Shindell, D. T.,  
925 Sillman, S., Skeie, R. B., Spracklen, D., Stavrou, T., Steenrod, S. D., Takemura, T., Tiitta, P.,  
926 Tilmes, S., Tost, H., van Noije, T., van Zyl, P. G., von Salzen, K., Yu, F., Wang, Z., Wang, Z.,  
927 Zaveri, R. A., Zhang, H., Zhang, K., Zhang, Q., and Zhang, X.: The AeroCom evaluation and  
928 intercomparison of organic aerosol in global models, *Atmos. Chem. Phys.*, 14, 10845-10895,  
929 doi:10.5194/acp-14-10845-2014, 2014.

930 Tsimpidi, A. P., Karydis, V. A., Zavala, M., Lei, W., Molina, L. T., Ulbrich, I., Jimenez, J. L.,  
931 and Pandis, S. N.: Evaluation of the volatility basis-set approach for the simulation of organic  
932 aerosol formation in the Mexico City metropolitan area, *Atmos. Chem. Phys.*, 10, 525-546,  
933 doi:10.5194/acp-10-525-2010, 2010.

934 Turpin, B. J. and Lim, H.-J.: Species Contributions to PM<sub>2.5</sub> Mass Concentrations: Revisiting  
935 Common Assumptions for Estimating Organic Mass, *Aerosol Sci. Technol.*, 35, 602-610,  
936 doi:10.1080/02786820119445, 2001.

937 Volkamer, R., Jimenez, J. L., San Martini, F., Dzepina, K., Zhang, Q., Salcedo, D., Molina, L.  
938 T., Worsnop, D. R., and Molina, M. J.: Secondary organic aerosol formation from anthropogenic

939 air pollution: Rapid and higher than expected, *Geophys. Res. Lett.*, 33, L17811,  
940 doi:10.1029/2006gl026899, 2006.

941 Worton, D. R., Surratt, J. D., LaFranchi, B. W., Chan, A. W. H., Zhao, Y., Weber, R. J., Park, J.-  
942 H., Gilman, J. B., de Gouw, J., Park, C., Schade, G., Beaver, M., Clair, J. M. S., Crounse, J.,  
943 Wennberg, P., Wolfe, G. M., Harrold, S., Thornton, J. A., Farmer, D. K., Docherty, K. S.,  
944 Cubison, M. J., Jimenez, J.-L., Frossard, A. A., Russell, L. M., Kristensen, K., Glasius, M., Mao,  
945 J., Ren, X., Brune, W., Browne, E. C., Pusede, S. E., Cohen, R. C., Seinfeld, J. H., and  
946 Goldstein, A. H.: Observational Insights into Aerosol Formation from Isoprene, *Environ. Sci.*  
947 *Technol.*, 47, 11403-11413, doi:10.1021/es4011064, 2013.

948 Xu, L., Guo, H., Boyd, C. M., Klein, M., Bougiatioti, A., Cerully, K. M., Hite, J. R., Isaacman-  
949 VanWertz, G., Kreisberg, N. M., Knote, C., Olson, K., Koss, A., Goldstein, A. H., Hering, S. V.,  
950 de Gouw, J., Baumann, K., Lee, S.-H., Nenes, A., Weber, R. J., and Ng, N. L.: Effects of  
951 anthropogenic emissions on aerosol formation from isoprene and monoterpenes in the  
952 southeastern United States, *Proc. Nat. Acad. Sci.*, 112, 37-42, doi:10.1073/pnas.1417609112,  
953 2015a.

954 Xu, L., Kollman, M. S., Song, C., Shilling, J. E., and Ng, N. L.: Effects of NO<sub>x</sub> on the Volatility  
955 of Secondary Organic Aerosol from Isoprene Photooxidation, *Environ. Sci. Technol.*, 48, 2253-  
956 2262, doi:10.1021/es404842g, 2014.

957 Xu, L., Suresh, S., Guo, H., Weber, R. J., and Ng, N. L.: Aerosol characterization over the  
958 southeastern United States using high-resolution aerosol mass spectrometry: spatial and seasonal  
959 variation of aerosol composition and sources with a focus on organic nitrates, *Atmos. Chem.*  
960 *Phys.*, 15, 7307-7336, doi:10.5194/acp-15-7307-2015, 2015b.

961 Yeh, G. K. and Ziemann, P. J.: Gas-wall partitioning of oxygenated organic compounds:  
962 Measurements, structure-activity relationships, and correlation with gas chromatographic  
963 retention factor, *Aerosol Sci. Technol.*, 49, 727-738, doi:10.1080/02786826.2015.1068427,  
964 2015.

965 Zhang, Q., Jimenez, J. L., Canagaratna, M. R., Allan, J. D., Coe, H., Ulbrich, I., Alfarra, M. R.,  
966 Takami, A., Middlebrook, A. M., Sun, Y. L., Dzepina, K., Dunlea, E., Docherty, K., DeCarlo, P.  
967 F., Salcedo, D., Onasch, T., Jayne, J. T., Miyoshi, T., Shimojo, A., Hatakeyama, S., Takegawa,  
968 N., Kondo, Y., Schneider, J., Drewnick, F., Borrmann, S., Weimer, S., Demerjian, K., Williams,  
969 P., Bower, K., Bahreini, R., Cottrell, L., Griffin, R. J., Rautiainen, J., Sun, J. Y., Zhang, Y. M.,  
970 and Worsnop, D. R.: Ubiquity and dominance of oxygenated species in organic aerosols in  
971 anthropogenically-influenced Northern Hemisphere midlatitudes, *Geophysical Research Letters*,  
972 34, L13801, doi:10.1029/2007GL029979, 2007.

973 Zhang, X., Cappa, C. D., Jathar, S. H., McVay, R. C., Ensberg, J. J., Kleeman, M. J., and  
974 Seinfeld, J. H.: Influence of vapor wall loss in laboratory chambers on yields of secondary  
975 organic aerosol, *Proc. Nat. Acad. Sci.*, 111, 5802-5807, doi:10.1073/pnas.1404727111, 2014.

976 Zhang, X., Schwantes, R. H., McVay, R. C., Lignell, H., Coggon, M. M., Flagan, R. C., and  
977 Seinfeld, J. H.: Vapor wall deposition in Teflon chambers, *Atmos. Chem. Phys.*, 15, 4197-4214,  
978 doi:10.5194/acp-15-4197-2015, 2015.

979 Zhao, Y., Hennigan, C. J., May, A. A., Tkacik, D. S., de Gouw, J. A., Gilman, J. B., Kuster, W.  
980 C., Borbon, A., and Robinson, A. L.: Intermediate-Volatility Organic Compounds: A Large

981 Source of Secondary Organic Aerosol, *Environ. Sci. Technol.*, 48, 13743-13750,  
982 doi:10.1021/es5035188, 2014.

983 Ziemann, P. J. and Atkinson, R.: Kinetics, products, and mechanisms of secondary organic  
984 aerosol formation, *Chem. Soc. Rev.*, 41, 6582-6605, doi:10.1039/C2CS35122F, 2012.

985 Zotter, P., El-Haddad, I., Zhang, Y., Hayes, P. L., Zhang, X., Lin, Y.-H., Wacker, L., Schnelle-  
986 Kreis, J., Abbaszade, G., Zimmermann, R., Surratt, J. D., Weber, R., Jimenez, J. L., Szidat, S.,  
987 Baltensperger, U., and Prévôt, A. S. H.: Diurnal cycle of fossil and nonfossil carbon using  
988 radiocarbon analyses during CalNex, *J. Geophys. Res.-Atmos.*, 119, 6818-6835,  
989 doi:10.1002/2013JD021114, 2014.

990

991 **Table 1.** Model performance metrics determined for the three simulation groupings (SOM-no, SOM-low and SOM-high) for the low-  
 992 NO<sub>x</sub>, high-NO<sub>x</sub> and average parameterizations for STN and IMPROVE sites in SoCAB and the eastern US. Fractional bias is calculated  
 993 as  $2(C_{OA,sim}-C_{OA,obs})/(C_{OA,sim}+C_{OA,obs})$  and NMSE as  $abs[(C_{OA,sim}-C_{OA,obs})^2/(C_{OA,sim}\times C_{OA,obs})]$ , and the reported values are the averages  
 994 over all data points as percentages. Note that a negative fractional bias indicates observed [SOA] > simulated [SOA], i.e. that the  
 995 simulations are underpredicting.  $\rho_c$  are the concordance correlation coefficients from Eqn. 3.

996

Simulation	NO <sub>x</sub> parameterization	Southern California						Eastern US					
		STN <sup>a</sup>			IMPROVE <sup>b</sup>			STN <sup>a</sup>			IMPROVE <sup>b,c</sup>		
		Frac. Bias	NMSE	$\rho_c$	Frac. Bias	NMSE	$\rho_c$	Frac. Bias	NMSE	$\rho_c$	Frac. Bias	NMSE	$\rho_c$
SOM-no	low	-70	88	0.03	-75	114	0.36	-81	206	0.04	-55	105	0.31
	high	-61	69	0.02	-60	85	0.41	-58	166	0.12	-24	84	0.48
	average	-65	78	0.02	-67	97	0.39	-68	180	0.08	-38	89	0.43
SOM-low	low	-52	64	- 0.21	-45	65	0.36	-26	154	0.08	15	85	0.15
	high	-39	49	- 0.29	-27	47	0.27	-4	171	0.07	38	128	0.10
	average	-45	55	- 0.25	-36	54	0.32	-14	160	0.08	28	105	0.12
SOM-high	low	-25	51	- 0.03	-8	46	0.44	26	236	0.15	69	189	0.40
	high	-10	38	- 0.08	16	43	0.46	45	298	0.15	86	295	0.25
	average	-17	43	- 0.05	5	42	0.46	36	265	0.16	79	241	0.31

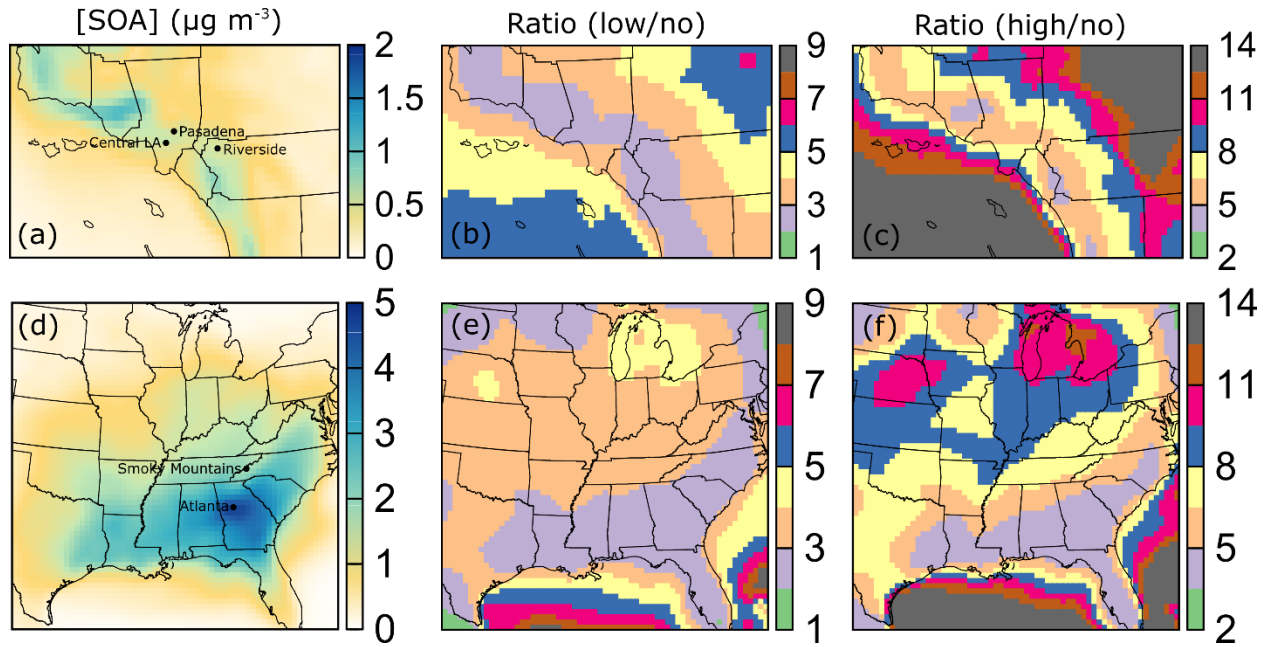
<sup>a</sup> Observed [OA] for STN sites estimated as 1.6([OC] – 0.5 μg m<sup>-3</sup>)

<sup>b</sup> Observed [OA] for IMPROVE sites estimated as 2.1[OC].

<sup>c</sup> Observed [OA] may be biased low by ~25% in the SE US summer due to evaporation after sampling (Kim et al., 2015).

997

998



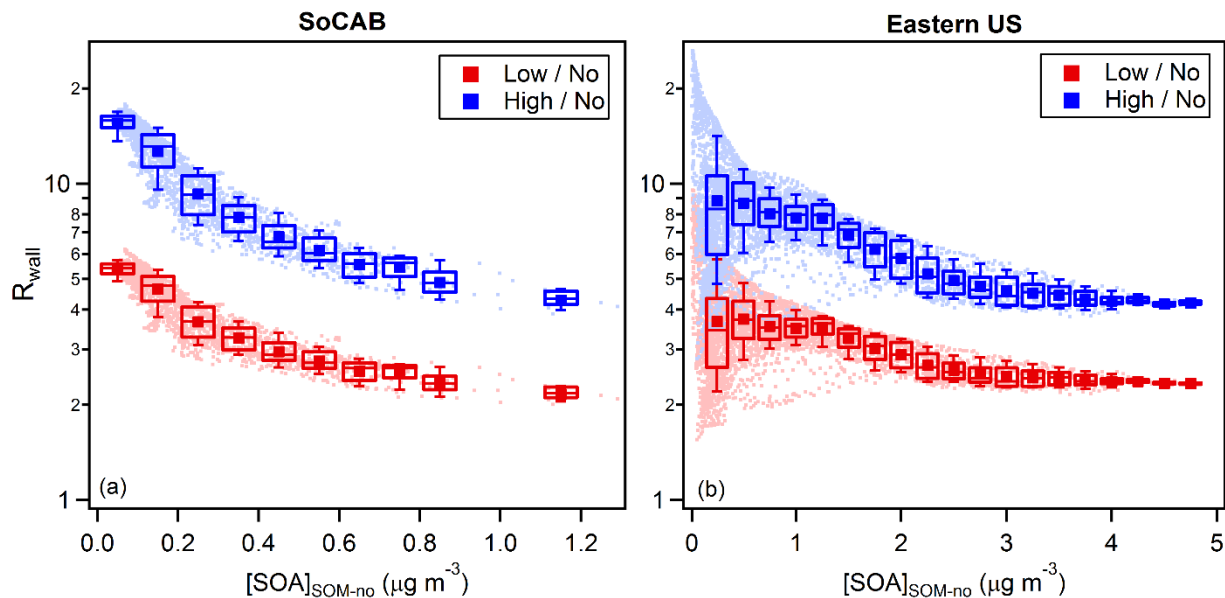
1000

1001 **Figure 1.** 14-day averaged SOA concentrations, in  $\mu\text{g m}^{-3}$ , for (a) SoCAB and (d) the eastern US  
 1002 for the SOM-no simulations. The averaging time periods are from July 20<sup>th</sup> to August 2<sup>nd</sup>, 2005  
 1003 for SoCAB and from August 20<sup>th</sup> to September 2<sup>nd</sup>, 2006 for the eastern US. Panels (b,e) show the  
 1004 ratio between the SOA concentrations for the SOM-low and the SOM-no simulations and Panels  
 1005 (c,f) show the ratio between the SOM-high and SOM-no simulations. Results shown in all panels  
 1006 are the average of the low- and high-NO<sub>x</sub> simulations. Note that the color scale for the absolute  
 1007 SOA concentration is continuous whereas the color scale in the ratio plots is discrete.

1008

1009

1010



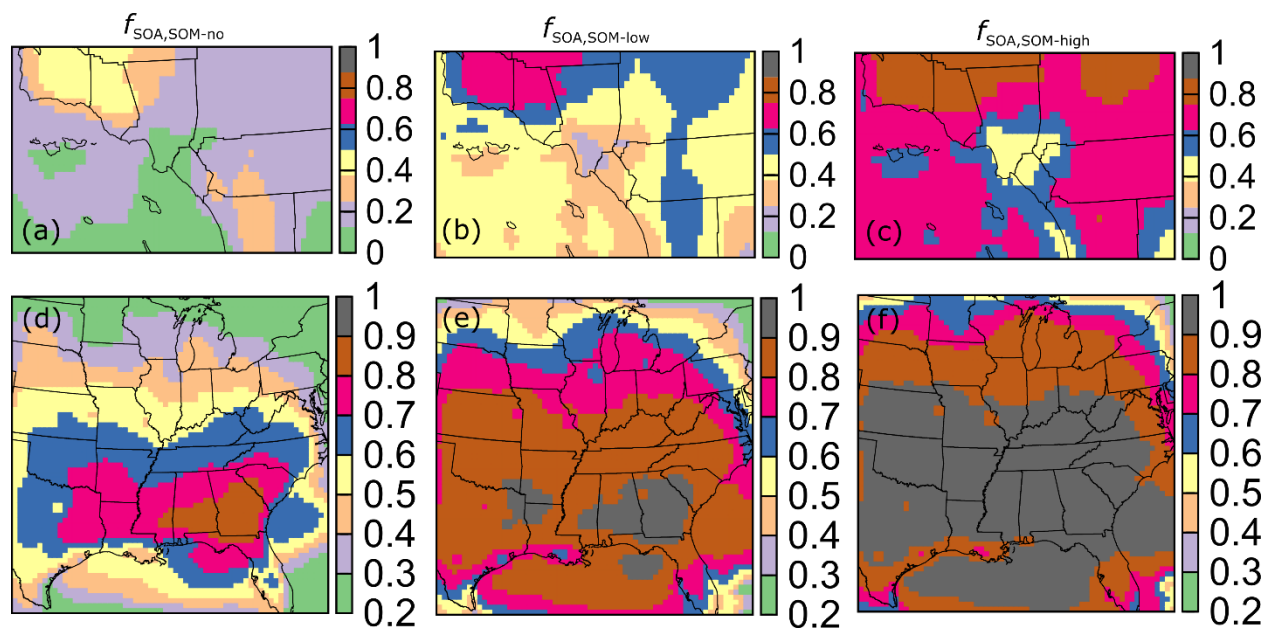
1011

1012 **Figure 2.** Variation of the ratio between simulated SOA concentrations from SOM-low (red) and  
1013 SOM-high (blue) simulations to SOM-no simulations for (a) SoCAB and (b) the eastern US as a  
1014 function of the absolute SOA concentration from the SOM-no simulations. Results shown are the  
1015 average of the low- and high- $NO_x$  simulations. Individual data points are shown along with box  
1016 and whisker plots.

1017

1018

1019



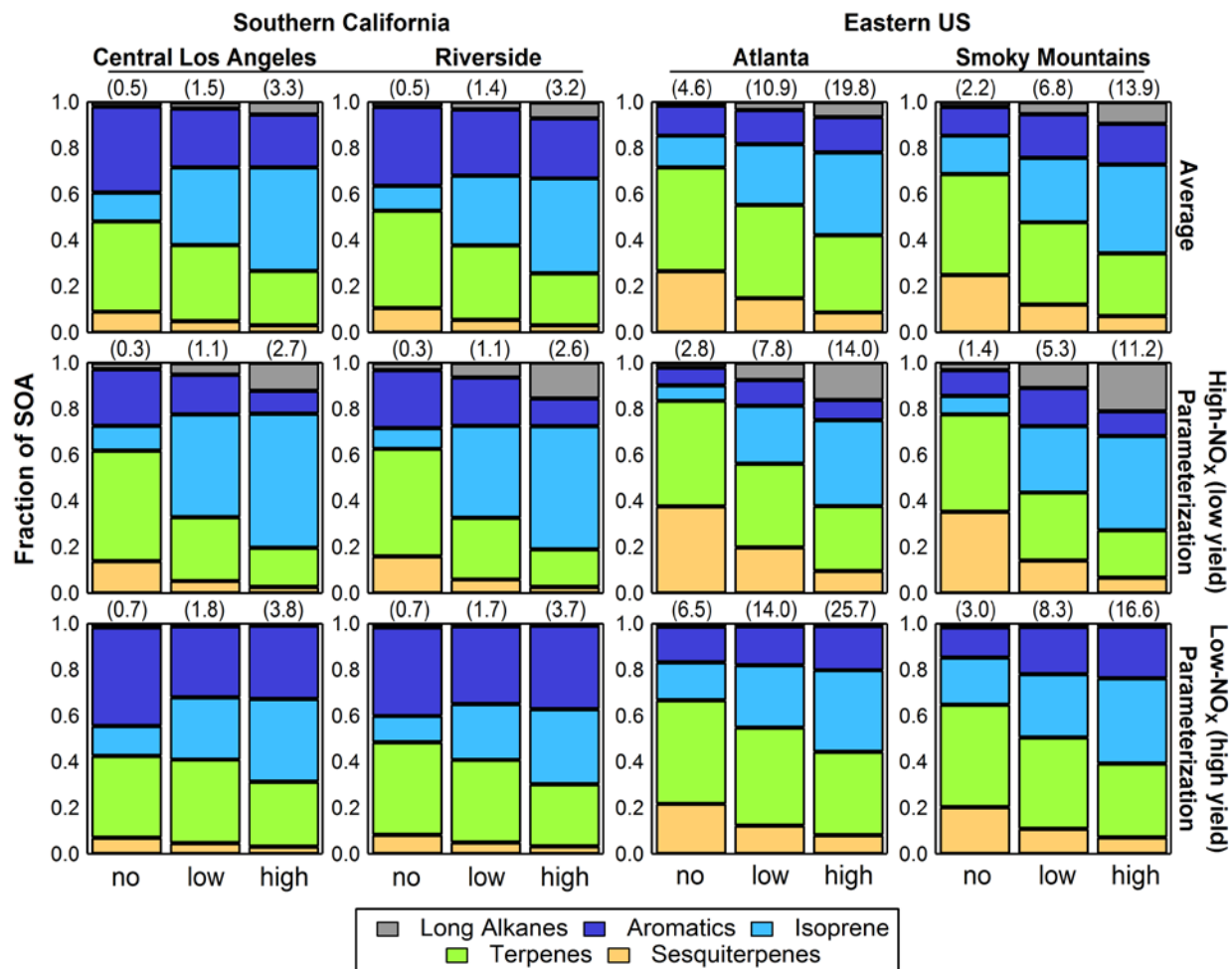
1020

1021 **Figure 3.** 14-day averaged  $f_{\text{SOA}}$ , the ratio between SOA and total OA concentrations, for (top  
1022 panels, a, b, c) SoCAB and (bottom panels, d, e, f) the eastern US for the (a, d) SOM-no, (b, e)  
1023 SOM-low and (c, f) SOM-high simulations.

1024

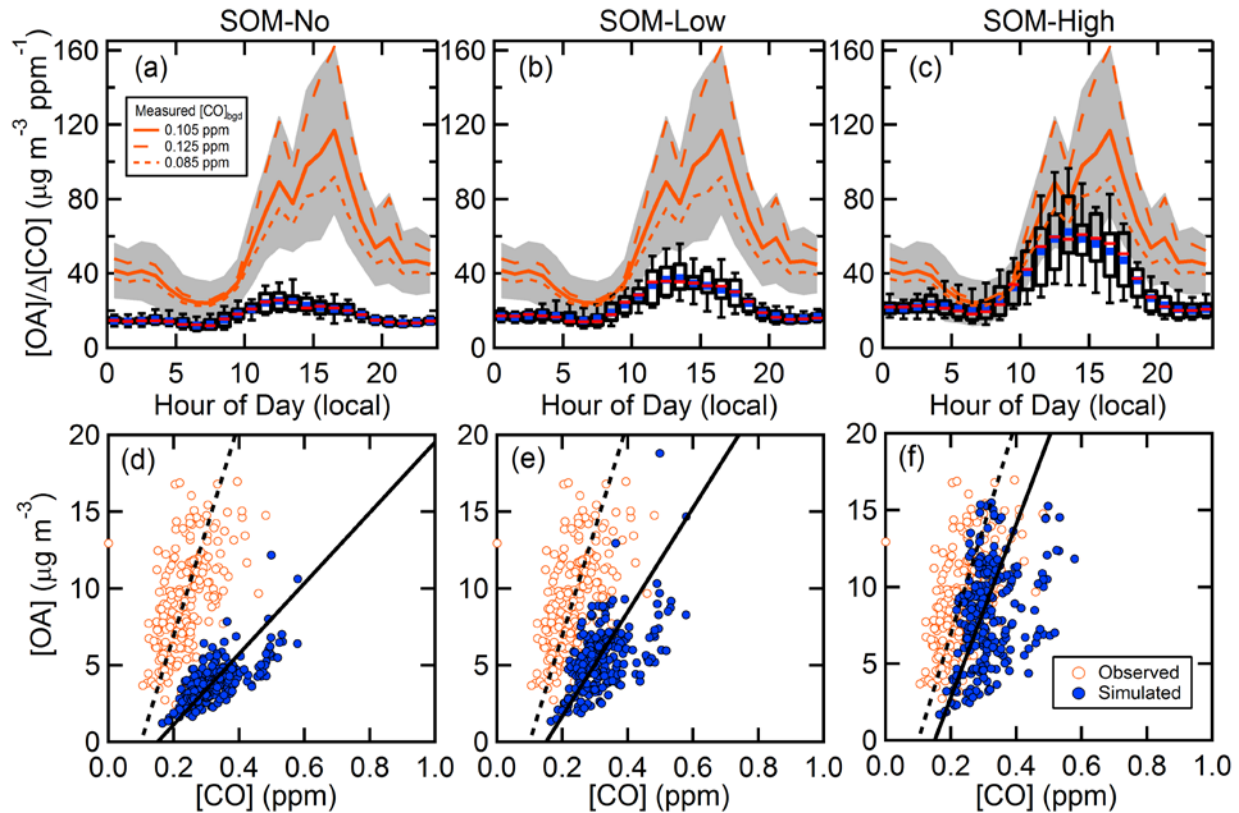
1025

1026



1028

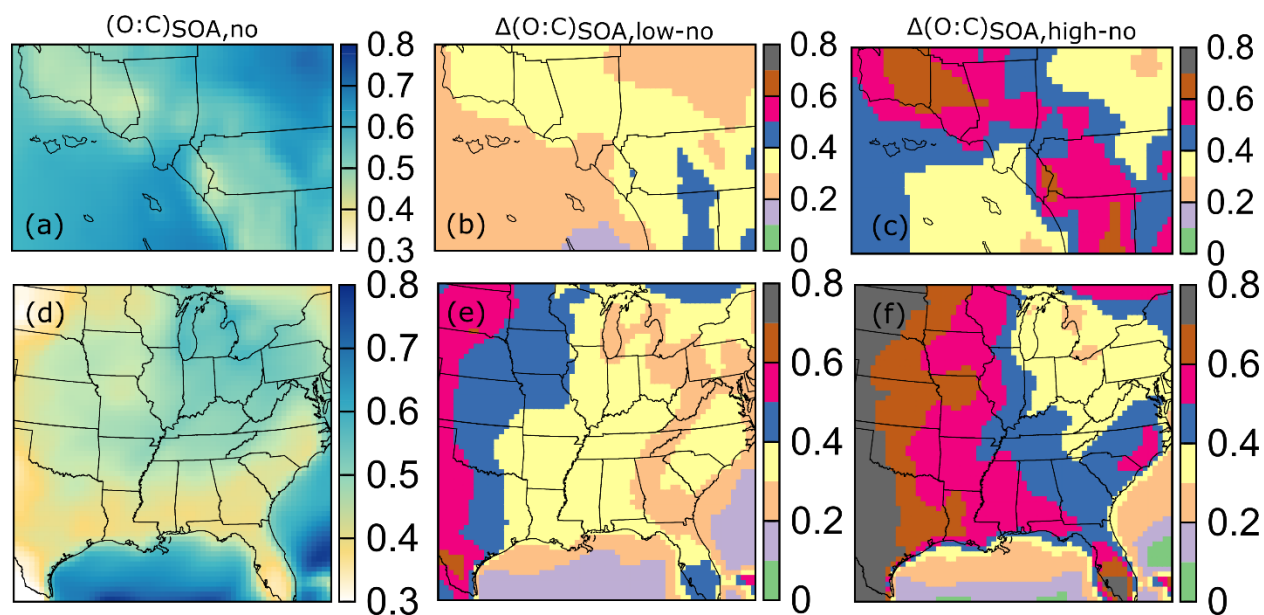
1029 **Figure 4.** Bar charts showing the fractional contribution from the various VOC precursor classes  
 1030 to the total simulated SOA for two locations in SoCAB (central Los Angeles and Riverside) and  
 1031 two in the eastern US (Atlanta and the Smoky Mountains). Results are shown for (top) average,  
 1032 (middle) high-NO<sub>x</sub>, low-yield and (bottom) low-NO<sub>x</sub>, high-yield simulations. Each panel shows  
 1033 results from the 14-day average (left-to-right) SOM-no, SOM-low and SOM-high simulations. The  
 1034 average SOA concentration (in  $\mu\text{g m}^{-3}$ ) is for each location and simulation is given in parentheses  
 1035 above each panel.



1036

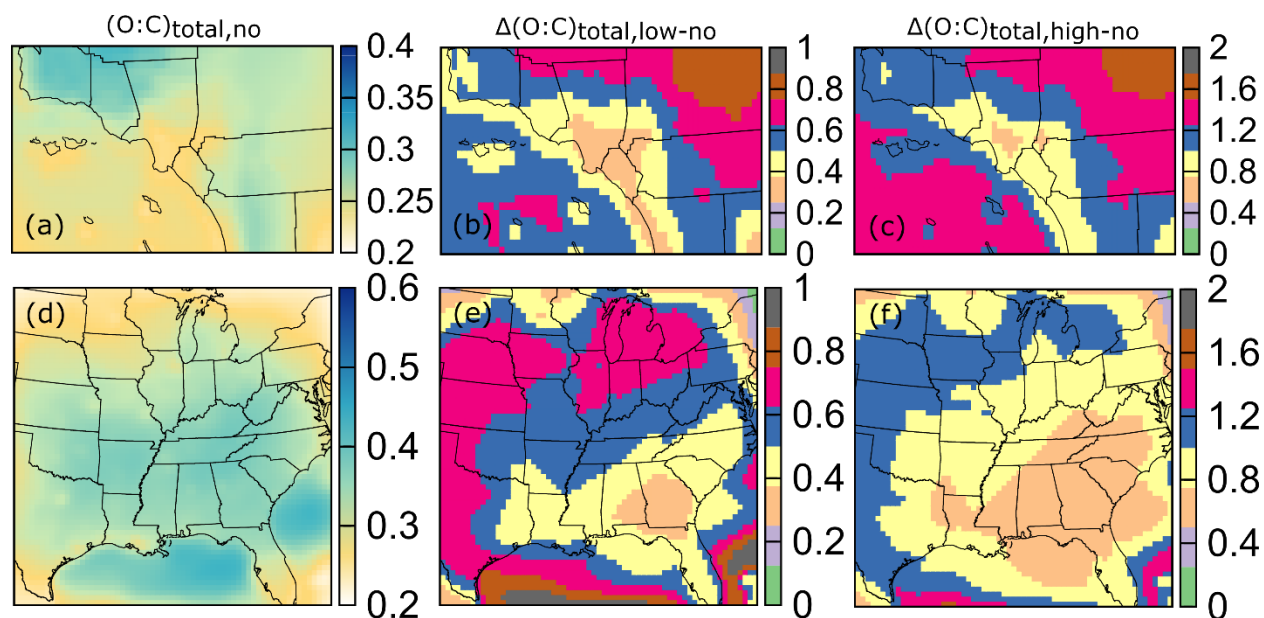
1037 **Figure 5.** Simulated and observed diurnal profiles for the OA/ΔCO ratio (top panels) at Riverside,  
 1038 CA during the SOAR-2005 campaign for (a) SOM-no, (b) SOM-low and (c) SOM-high  
 1039 simulations. For the observations, the mean (solid orange line) and the 1σ variability range (grey  
 1040 band) are shown for [CO]<sub>bgd</sub> = 0.105 ppm, and only mean values are shown for [CO]<sub>bgd</sub> = 0.085  
 1041 ppm (short dashed orange line) and [CO]<sub>bgd</sub> = 0.125 ppm (long dashed orange line). For the  
 1042 simulations, box and whisker plots are shown with the median (red –), mean (blue squares), lower  
 1043 and upper quartile (boxes), and 9<sup>th</sup> and 91<sup>st</sup> percentile (whiskers). The bottom panels (d-f) show  
 1044 scatter plots of [OA] versus [CO] for both the ambient measurements (open orange circles) and  
 1045 for the model results (blue circles) for daytime hours (10 am – 8 pm). The lines are linear fits  
 1046 where the x-axis intercept has been constrained to go through the assumed [CO]<sub>bgd</sub> (dashed =  
 1047 observed; solid = model). The derived slopes are 69 ± 2 (observed), 23.0 ± 0.4 (SOM-no), 34.0 ±  
 1048 0.8 (SOM-low) and 55 ± 2 (SOM-high) μg m<sup>-3</sup> ppm<sup>-1</sup> and where the uncertainties are fit errors.

1049



1050  
 1051 **Figure 6.** 14-day averaged O:C atomic ratios for SOA for (a) SoCAB and (d) the eastern US for  
 1052 the SOM-no simulations. The difference in O:C between the SOM-low or SOM-high and SOM-  
 1053 no simulations, termed  $\Delta(\text{O:C})$ , is shown in panels (b-c) for SoCAB and (e-f) for the eastern US.  
 1054

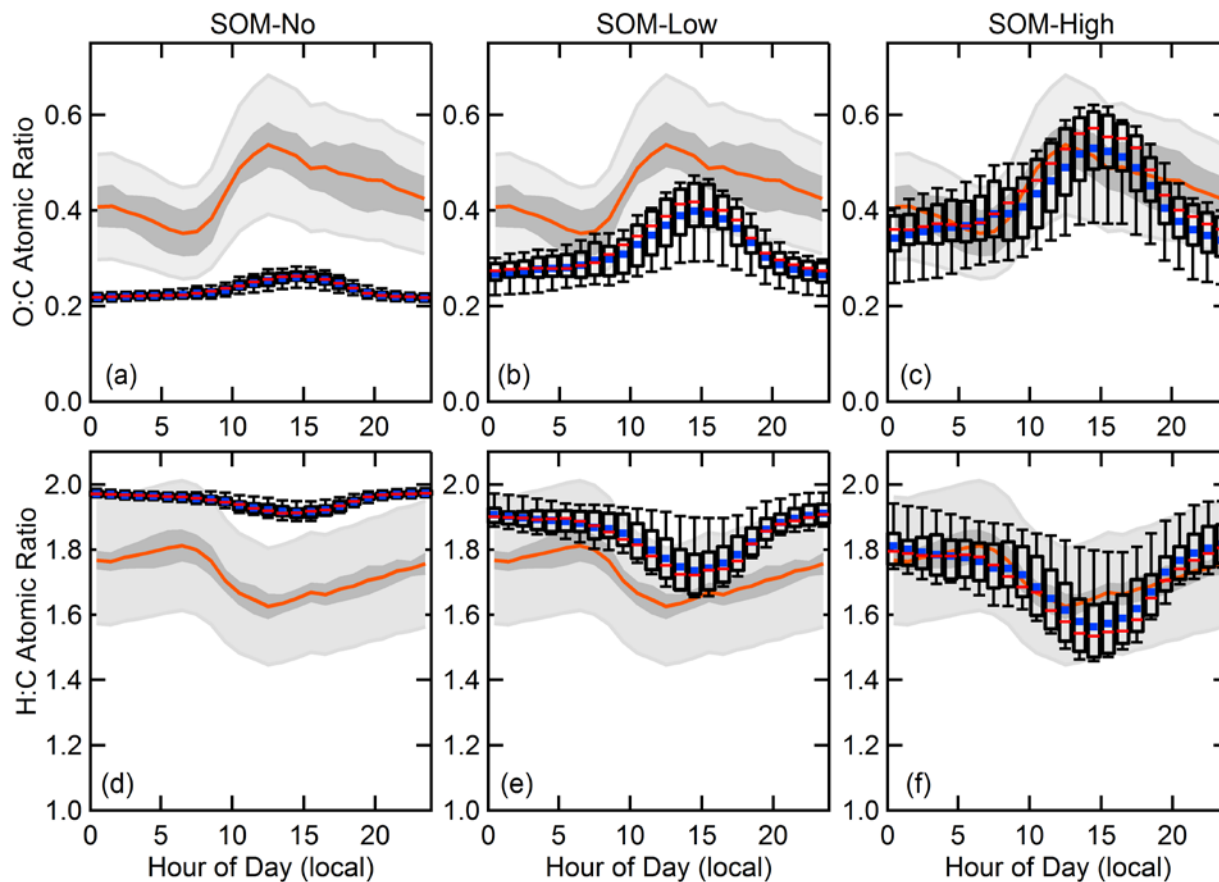
1055



1056

1057 **Figure 7.** 14-day averaged O:C atomic ratios for total OA (POA + SOA) for (a) SoCAB and (d)  
1058 the eastern US for the SOM-no simulations. The normalized difference in O:C,  $\Delta(\text{O:C})$ , between  
1059 the SOM-low or SOM-high and SOM-no simulations, where  $\Delta(\text{O:C})$  is defined as  
1060  $((\text{O:C})_{\text{SOM-low/high}} - (\text{O:C})_{\text{SOM-no}}) / (\text{O:C})_{\text{SOM-no}}$ , is shown in panels (b-c) for SoCAB and (e-f) for the  
1061 eastern US. In all cases, the O:C for POA was assumed to be 0.2.

1062



1064

1065 **Figure 8.** Simulated and observed diurnal profiles for the total OA O:C (panels a, b, c) and H:C  
 1066 (panels d, e, f) atomic ratios at Riverside, CA during the SOAR-2005 campaign for (a, d) SOM-  
 1067 no, (b, e) SOM-low and (c, f) SOM-high simulations. For the observations, the mean (orange line)  
 1068 and the  $1\sigma$  variability range (dark grey band) are shown along with bands indicating the  
 1069 measurement uncertainty (light grey band), taken as  $\pm 28\%$  for O:C and  $13\%$  for H:C (Canagaratna  
 1070 et al., 2015). Observed values have been corrected according to Canagaratna et al. (2015). For the  
 1071 simulations, box and whisker plots are shown with the median (red –), lower and upper quartile  
 1072 (boxes), and 9<sup>th</sup> and 91<sup>st</sup> percentile (whiskers). For reference, the assumed O:C for POA was 0.2  
 1073 and for H:C was 2.0.

1074